



ENGINEERING APPLICATIONS OF ELECTRO-RHEOLOGICAL FLUIDS

Tam Dinh Truong

A thesis
submitted in total fulfillment
of the requirements for the degree of
Master of Engineering

School of the Built Environment – Mechanical Engineering
Victoria University of Technology

Footscray Campus
PO BOX 14428 MCMC
Melbourne, Victoria 8001
Australia

September, 2000



FTS THESIS

620.11297 TRU

30001006992277

Truong, Tam Dinh

Engineering applications of
electro-rheological fluids

Abstract

The use of electro-rheological (ER) fluids is relatively new in engineering applications. ER fluids can change from liquid to solid-like gel under an electrical field, and this change takes place within milliseconds. The change is reversible once the electrical field is removed. This thesis is an experimental investigation to deal with three particular engineering applications of ER fluids. The first application is improving the vibration control characteristics of a conventional tuned absorber using an ER fluid as the working fluid of the absorber. The second application is to demonstrate the same ER fluid's ability to couple two discs for power transmission. This concept is similar to the operation of a clutch or direct coupling device between rotating machinery. The third application is of more exploratory type. It deals with switching the shape of an airfoil in flight between two different profiles. The purpose of such switching action is to exploit different aerodynamic properties of two different profiles, ultimately leading to a simple design for improved flight safety.

TABLE OF CONTENTS

Abstract	ii
List of Tables	v
List of Figures	vi
Chapter 1 Electro-Rheological Fluids in Engineering Applications	
1.1 Introduction	1
1.2 Discovery of ER effect	2
1.3 Earlier Engineering Applications	3
1.3.1 Shearing Mode	4
1.3.2 Valve Mode	5
1.4 Two Examples of ER Dampers	6
1.5 Significance and Thesis Structure	9
Chapter 2 A Variable Damping Tuned Absorber with ER Fluid for Transient Resonance of Light Structures	
2.1 Introduction	12
2.2 Sloshing Absorber with an ER Fluid	15
2.3 Energy Dissipation with Sloshing ER Fluid	18
2.4 Numerical Predictions	22
2.5 Experiments	30
2.6 Conclusions	37
Chapter 3 Experimental Demonstration of an ER Clutch	
3.1 Introduction	38
3.2 Experimental Setup	39
3.3 Results	44

3.4 Viscosity Measurement	47
3.5 Conclusions	52
Chapter 4 Airfoil Section Modifications with ER Fluid	
4.1 Introduction	53
4.2 Aerodynamic Characteristics a Two-Dimensional Airfoil	54
4.3 Basic Stages of Flight	54
4.3.1 Take-off	55
4.3.2 Climb	55
4.3.3 Level Flight	56
4.3.4 Glide and Landing	57
4.4 Aerodynamic Characteristics of NACA0012 and NACA0006	58
4.5 Laboratory Prototype	63
4.6 Conclusions	72
Chapter 5 Conclusions	74
References	76
Appendix A Software to Simulate Dynamic Response of a Tuned Absorber	83

List of Tables

page

Table 2.1. Structural parameters of the experimental setup when each component is tested alone.

20

Table A.1. Example input with a sinusoidal excitation.

81

List of Figures	page
Figure 1.1. a) Electric field strength below 1kV/mm, and b) Electric field strength above 2kV/mm	2
Figure 1.2. Shear Mode Type Damper (Brennan et al., 1995).	4
Figure 1.3. Valve Mode Type Damper (Brennan et al., 1995).	6
Figure 1.4. Parallel Plate ER fluid Clutch. (Carlson et al.,1989).	6
Figure 1.5. a) ER damper. b) The overall view of the piping model (Otani et al.,1994).	8
Figure 1.6. Typical displacement spectrum (Otani et al., 1994).	9
Figure 2.1. (a) A simple mechanical oscillator with a tuned absorber. (b) Response of the primary structure for different excitation frequencies. ζ is the critical damping ratio of the absorber.	12
Figure 2.2. Sloshing absorber attached on the primary structure to be controlled.	15
Figure 2.3. (a) Tuned absorber with variable damping. (b) Sloshing absorber with ER fluid to provide variable damping.	16
Figure 2.4. (a) Experimental setup. (b) and (c) typical decay histories of the structure with no voltage.	18 19
Figure 2.5. Displacement history of the primary structure with a constant ζ of (a) 0.02, (b) 0.05, (c) 0.20; and with a variable ζ of either (d) 0.05 or (e) 0.20 until 100 seconds and 0.02 after 100 seconds.	23
Figure 2.6. Same as in Figure 6, but for the tuned absorber.	24
Figure 2.7. Same as in Figure 6, but for an acceleration over 250 seconds.	27
Figure 2.8. Same as in Figure 7, but for an acceleration over 250 seconds.	28
Figure 2.9. (a) Schematic of the experimental setup where the experimental apparatus is the same as in Figure 5(a) with the addition of 6: Radio Spares - RS 266-985 dc electric motor with an unbalance disk.	30
Figure 2.9. (b) Photograph showing experimental setup (c) Photograph showing the sloshing container.	31

Figure 2.10. Experimentally observed displacement history of the primary structure with (a) full voltage, (b) no voltage and (c) no voltage until 100 seconds and then full voltage.	33
Figure 2.11. Same as in Figure 2.10, but for the tuned absorber.	35
Figure 3.1. Schematic diagram of the experiment setup.	40
Figure 3.2. Photograph of the ER clutch setup.	41
Figure 3.3. Photograph of the ER clutch.	41
Figure 3.4. Close up of the ER clutch.	42
Figure 3.5. Photograph of the ER clutch components.	42
Figure 3.6. Variation of the speed ratio with the applied voltage. ER fluid is 55% volume fraction, cornstarch in mineral oil.	44
Figure 3.7. A suggested bladed configuration of the input disk to increase the capacity for power transfer.	46
Figure 3.8. Schematic representation of the test rigs as a viscosity measuring device.	47
Figure 3.9. The configuration used in the derivation of the viscosity expression.	47
Figure 4.1. Cross-section of an airfoil.	53
Figure 4.2. Lift/Drag ratio versus angle of attack in general for an airfoil (Trevor, 1996).	56
Figure 4.3. Schematic diagram of the landing phase (Trevor, 1996).	57
Figure 4.4. Showing the standard profiles of (a) NACA0012 and (b) NACA0012.	58
Figure 4.5. (a) Lift coefficient (b) Drag coefficient (c) Moment coefficient of NACA0006 (\square) and NACA 0012 (\bullet) (Easterman, 1931).	60
Figure 4.6. (a) Lift coefficient, (b) Drag coefficient and (c) Moment coefficient.	62
Figure 4.7. Schematic diagram of the overall experimental setup.	64
Figure 4.8. (a) Drawing and (b) photograph of the leading edge.	67

Figure 4.9. Same as in Figure 4.8, but for the trailing edge.	68
Figure 4.10. One of the conductor plate sides.	69
Figure 4.11. Photograph of an airfoil section of NACA0006 without sealing jacket.	70
Figure 4.12. Photograph of an airfoil section of NACA0012 without sealing jacket.	70
Figure 4.13. Photograph of the airfoil section of NACA0006 with sealing jacket.	71
Figure 4.14. Photograph of the airfoil section of NACA0012 with sealing jacket.	71
Figure A.1. A simple mechanical oscillator with a tuned absorber.	79
Figure A.2. Execution of the program in the Matlab command window environment.	82
Figure A.3. Example output of the displacement history of the primary structure with no damping.	83
Figure A.4. Example output of the displacement history of the absorber with no damping.	83

Chapter 1

ELECTRO-RHEOLOGICAL FLUIDS IN ENGINEERING APPLICATIONS

1.1 Introduction

Application of controllable fluids in structures is a relatively new area which only in the early 1980s began to be explored. Controllable fluids of interest in this study are materials that respond to an applied electric field, with a dramatic change in rheological behavior. These materials are commonly referred as Electro-Rheological (ER) fluids. The essential characteristic of ER fluids is their ability to change from free-flowing, linear viscous liquids to semi-solids having controllable shear strength when exposed to an electric field (Housner 1997). This change typically takes place over milliseconds, and it is completely reversible.

These “smart materials” offer flexibility in altering the response of a structure when confronted with unexpected or changing environments. Of particular importance to motion control is the ease with which damping and stiffness properties of ER fluid devices can be varied with the application of an appropriate electric field.

ER fluids consist of a base fluid, usually some type of low viscosity insulating liquid, such as mineral and silicone oils, mixed with 1-10 μm diameter non-conductive particles, such as corn starch, gypsum and lithium salt. The behavior of an ER fluid is dependent upon the distance between the two electrodes as well as the magnitude of the potential applied on the electrodes.

At low field strengths (or at no electric potential), as shown in Figure 1.1(a), an ER fluid has a viscous liquid state. The particles are randomly distributed in the suspension oil. At electrical potentials of sufficient strength, on the other hand, the suspended particles align to form chains from one electrode to the other. Chains form as a result of the strong electro-static attraction force between the particles. At field strengths above 2kV/mm, as shown in Figure 1.1(b), an ER fluid behaves more like a solid, since a significant number of particle chains has been formed. When the electric field strength reaches a critical value, an ER fluid changes from liquid to almost solid, and it has high yield strength (Gouzhi et al., 1995). Upon further increase in the field strength, chains become thicker, and the corresponding yield strength increases (Housner, 1997; Gouzhi et al.,1995; Tsukiji and Tanaka, 1996; Suresh et al., 1994; and Berg et al., 1996).

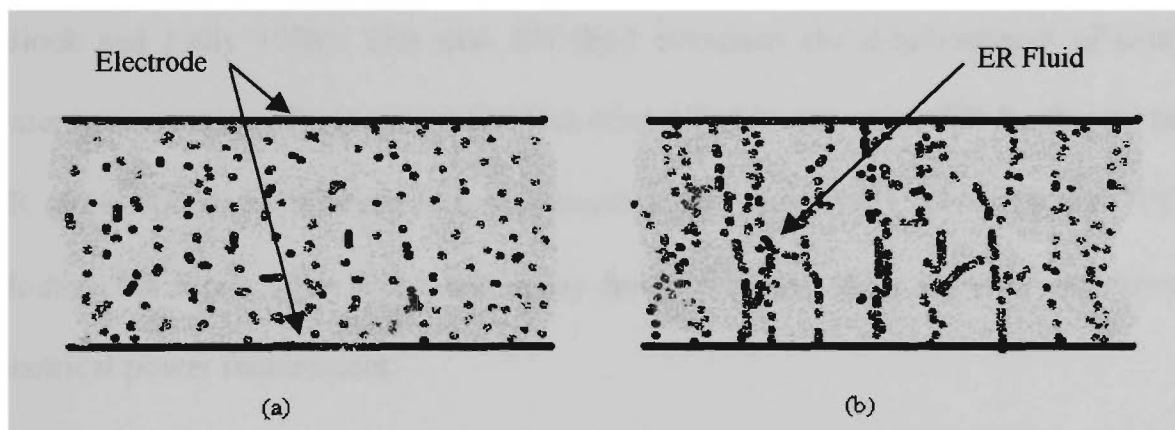


Figure 1. Showing an ER fluid (a) with no electric field and b) with an electric field strength above 2kV/mm.

1.2 Discovery of ER Effect

W. M. Winslow discovered an ER fluid in 1949 (Winslow 1949). Winslow's early experiments provided a procedure to use powder dispersed in oil between conducting electrodes to give a demonstration of force transmitted through a fluid under the

influence of applied voltage. Early ER fluids usually contained water in the suspension. Water enhanced the conductivity of ER fluids. On the other hand, the presence of water restricted the working temperature range. Above 70°C, water evaporated, and hence, it reduced the ER effect. Below 0°C, water iced with a crystal lattice structure, and it lost its ability as an activator, again decreasing the ER effect. Without water, no appreciable shear force could be developed, while too much water produced large power demands and arcing across the electrodes as the sample became more conductive and caused easier electric breakdown (Gouzhi et al., 1995). Early ER fluids could not meet the requirements of practical applications, because their suspension particles settled quickly, and their rheological effect was relatively weak.

Block and Kelly developed a water-free semi conducting polymer substrate ER fluid (Block and Kelly 1988). This new ER fluid overcame the disadvantages of using water in suspension. Temperature had less of an effect in water-free ER fluids, and the ER effect still occurred even at temperatures higher than 100°C or lower than 0°C. Modern ER fluids after Block and Kelly have increased shear strength and lower electrical power requirement.

1.3 Early Engineering Applications

Traditionally, passive devices have been employed to shift natural frequencies and to introduce adequate damping into structures. These structures had to be heavy to give the required stiffness and damping to eliminate transient oscillation. More recently, the advantage of employing ER fluid as a medium to control structural oscillation has attracted many researchers (Brennan et al., 1995; Carlson and Duclos 1989; Otani et

al., 1994; and Bullough et al., 1994). It is the effortless way in which these materials can be used to make fast acting valves with no moving parts which has attracted the attention of the vibration control community and has provided the possibility of a cheap, reliable, alternative technology (Block and Kelly 1988). Brennan et al. investigated and compared the designs of two main classes of ER dampers, one which acts by shearing the otherwise stationary fluid, and the other which acts by pumping the fluid. These two classes are discussed briefly next.

1.3.1 Shearing Mode

In the shearing mode type of an ER damper, shown in Figure 1.2, the ER fluid is contained between one or more pairs of electrodes which are free to move parallel to each other (perpendicular to the electric field) such that the ER fluid is subjected to a uniform shear. In Figure 1.2, b and L are the electrode breadth and depth; h is the distance between the electrodes; E is the applied voltage; F is the total damping force force; and V is the relative velocity between the electrodes.

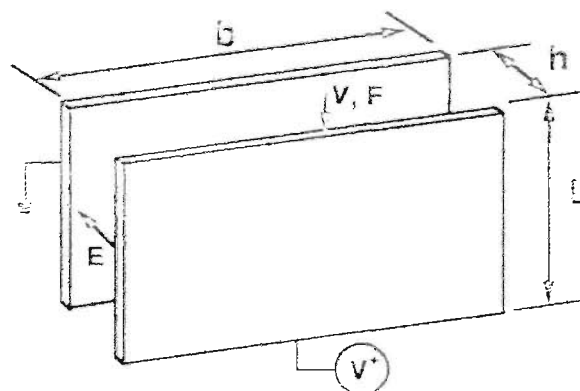


Figure 1.2. Shear mode type damper (Brennan et al.,1995).

There are two forces associated with this type of an ER damper: a passive force due to the viscosity of the fluid, F_V , and an active force due to the ER effect, F_C . The passive force F_V is present at all times, and it is dependent on the viscosity of the fluid and the geometric properties of the damper. When an electric field is applied, a static force F_C (due to the formation of suspended particles aligning themselves between electrodes), needs to be overcome before the motion can occur. This force F_C is equal to the product of the fluid yield strength and the area of one electrode, and it is independent of the velocity of the electrode plates. The total damping force of this type of an ER damper, F , is the summation of the two force components. The objective of this type of an ER damper is to provide a large ratio of on-field to off-field damping, through the ratio of the two forces: F_C and F_V . Such a large ratio consequently enables significantly different response from the ER unit with varying voltage.

1.3.2 Valve Mode

In the valve mode of operation, the ER fluid is squeezed between the electrodes as shown in Figure 1.3. Thus, the ER fluid is subjected to tension/compression and shear. If the ER fluid is squeezed between the electrodes in the absence of an electric field, it behaves like a Newtonian fluid. Consequently, a pressure drop, ΔP , arises at a volume flow rate, Q . This change in pressure across the valve is due to the viscosity of the ER fluid. However, when an electric field is applied, the ER fluid develops a yield stress, and the effect of this stress is to produce an additional pressure drop across the length of the two plates. The total damping force of this type of an ER damper is the summation of these two force components. In this mode, the

effectiveness of the device is the ratio of the two pressure drops across the valve with and without the ER effect.

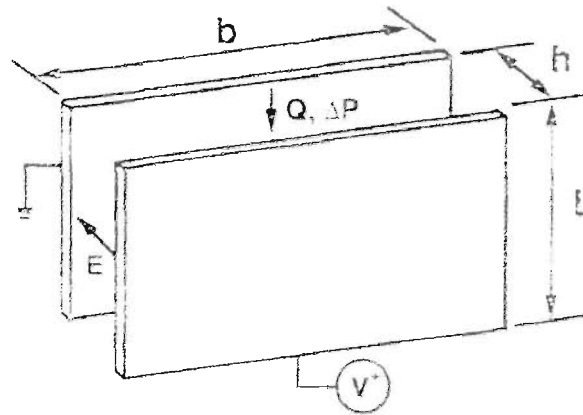


Figure 1.3. Valve mode type damper (Brennan et al., 1995).

1.4 Two Examples of ER Dampers.

The way in which an ER fluid is used in a vibration system greatly affects the vibration control capabilities of the ER fluid (Coulter et al., 1989). The rotary arrangement shown in Figure 1.4 was used in Carlson and Duclos (1989) to study the effect of an ER-fluid in dynamic vibration absorber. The rotating dynamic vibration absorber consists of the two parallel disc plates separated by a flat layer of ER fluid. This application is an example of using an ER fluid in shearing mode.

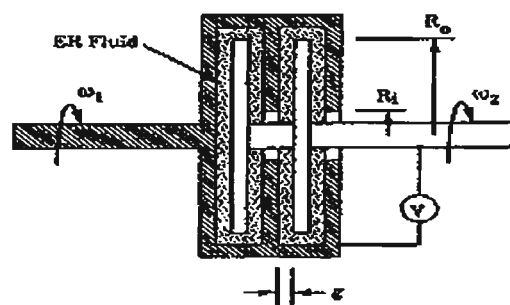


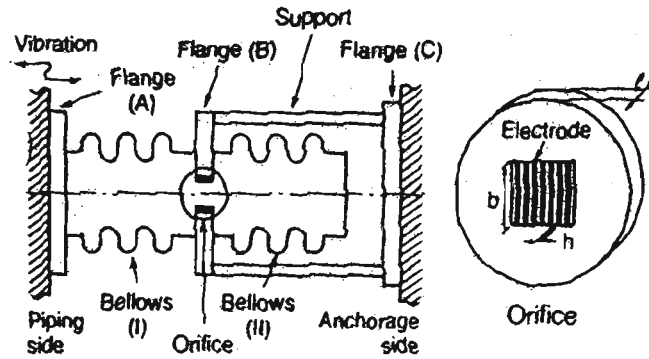
Figure 1.4. Parallel plate ER fluid rotating vibration absorber (Carlson and Duclos 1989).

In Figure 1.4, ω_1 and ω_2 are rotational speed of the input and output shafts, respectively. R_o is the radius of the rotating plates. g is the gap between electrodes. There are two torques associated with the ER damper shown in Figure 1.4: viscous torque T_V and ER torque T_E . The viscous torque, T_V , consists of the viscous force times the torque arm (radius). T_V is independent of the applied voltage and dependent only on the viscosity of the fluid. When the ER fluid is activated, assuming yielding takes place across the whole disc, then the torque required to produce yielding over an area is the ER torque T_E .

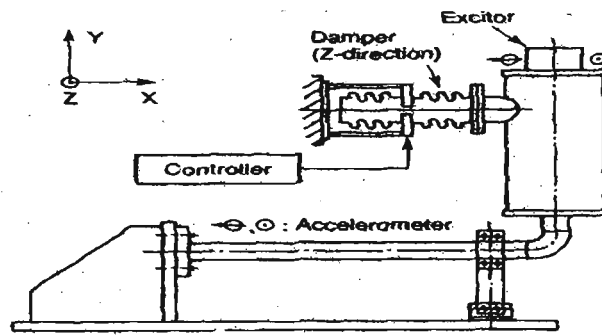
Another typical example of an ER damper is from Otani et al., 1994. In this reference, the valve mode type of an ER damper is used to control the response of a piping system, as shown in Figure 1.5. Commonly, piping supports such as mechanical snubbers or elasto-plastic dampers are effective in reducing the seismic response of piping systems in which the amplitudes of vibration are large. However, the unbalanced forces of pumps and the forces of internal fluid usually excite the piping system with a wide range of frequencies and small amplitudes so that common piping supports are not effective.

The valve mode type of ER damper shown in Figure 1.5 (a) consists of an orifice containing many slits at the center of flange B. The overall piping model is shown in Figure 1.5(b). ER fluid is contained within metal bellows. Flanges A and C are fixed to the vibrating pipe and anchor point, respectively. When the displacement of the piping system increases, the ER fluid within the metal bellows is pumped from bellow 1 to bellow 2. Viscous resistance of the ER fluid generates the damping force as it

moves through the orifice, and it can be controlled by varying the applied electric field.



(a)



(b)

Figure 1.5. (a) ER damper and (b) The overall view of the piping model

(Otani et al., 1994).

This type of an ER damper provides advantages because of its structure. It is very effective in suppressing small amplitude (less than 0.1mm) vibrations, because there is no gap or friction in the damper or its connecting parts. With an ER fluid as the internal fluid, the desired damping force can be easily obtained by varying the applied electric field.

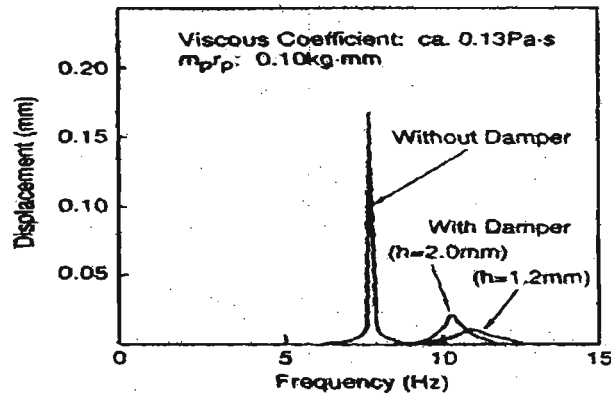


Figure 1.6. Typical displacement spectrum (Otani et al., 1994).

In Figure 1.6, each curve represents the pipe displacement with a different orifice gap. The results show that when the gap of the damper is decreased, the displacement of the piping system reduces dramatically, due to the effect of the change in the viscosity of the ER fluid when the electric field is applied.

1.5 Significance and Thesis Structure

The primary aim of this research project is to make the experimental research facilities available at Victoria University (VU) for research in Electro-Rheological (ER) fluids. The second outcome is to start the ER fluid research at VU with three practical and novel engineering applications. The first application is to use an Electro-Rheological fluid to control structural oscillations. The experimental details and results of this application are discussed in Chapter 2. Chapter 3 presents a new design to use an ER fluid as a coupling agent for power transmission. Chapter 4 deals with geometric changes of an airfoil in flight. The ER fluid used in this research project is corn starch and mineral oil. 40% volume fraction of corn starch is used in Chapter 2

to obtain high amplitude liquid sloshing when there is no voltage applied. 55% volume fraction is used in Chapter 3 to obtain high level of power transmission. Each chapter is presented as an independent entity with its literature review, discussion and conclusions.

Chapter 2

A VARIABLE DAMPING TUNED ABSORBER WITH ELECTRO-RHEOLOGICAL FLUID FOR TRANSIENT RESONANCE OF LIGHT STRUCTURES*

2.1 Introduction

Tuned vibration absorbers are simple and effective passive vibration control devices for lightly damped resonance structures. A simple system including a tuned absorber is shown in Figure 2.1(a) under the effect of a sinusoidal excitation “ $F_0 \sin \omega t$ ”. The primary structure to be controlled has a mass m_1 , viscous damping coefficient c_1 and stiffness k_1 , whereas m_2 , c_2 and k_2 represent the corresponding parameters of the tuned absorber. Vibration absorber is tuned by ignoring the damping in the system and by usually setting $(k_1 / m_1)^{1/2} = (k_2 / m_2)^{1/2}$, where the left and right sides of the equality represent the undamped resonance frequency of the structure (ω_1) and that of the absorber alone (ω_2), respectively (Hunt 1979 and Snowdon 1968). This simple equality ensures that the absorber is at resonance at the most critical frequency (at ω_1 or ω_2) of the structure to be controlled. In resonance, the absorber uses all the available energy in the system providing ideal control for the primary structure. The absorber which undergoes quite violent oscillations is considered to be expendable. It may also be shown readily that at the tuning frequency, the force of the absorber’s spring is of the same amplitude, but of opposite sign, as that of the external force $F_0 \sin \omega_2$.

* The material presented in this chapter has been accepted for publication as a full-paper in Journal of Sound and Vibration (Truong and Semercigil 2000)

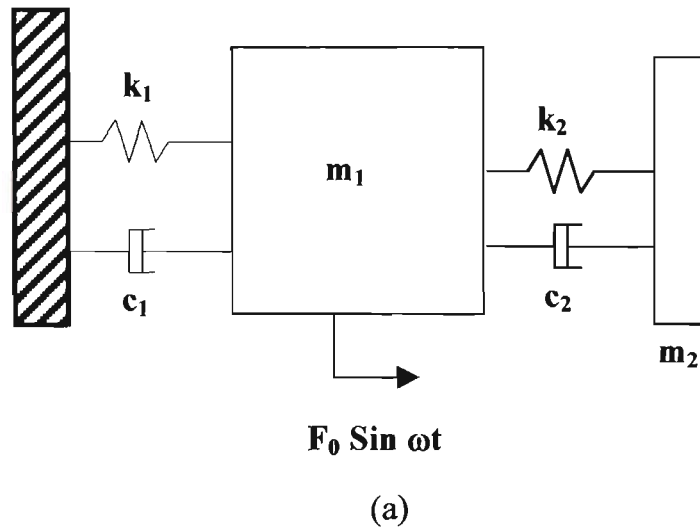


Figure 2.1 (a) A simple mechanical oscillator with a tuned absorber.

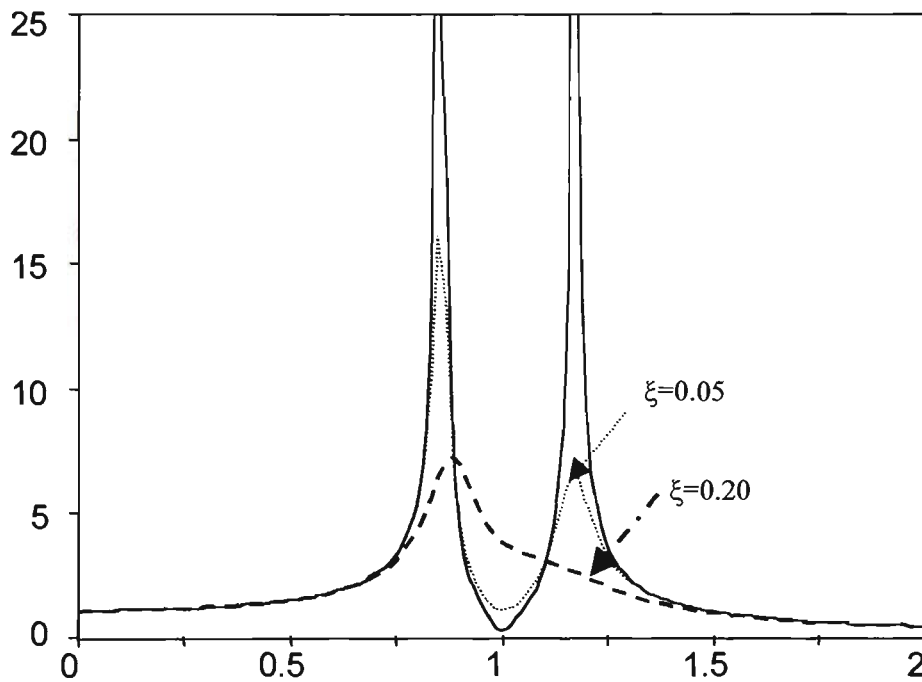


Figure 2.1 (b) Response of the primary structure for different excitation frequencies. ζ is the critical viscous damping ratio of the absorber.

In Figure 2.1(b), the steady state displacement amplitude of the undamped ($c_1 = 0$) primary structure, X_1 , is shown for different frequencies of the excitation $F_0 \sin \omega t$. The horizontal axis represents the non-dimensional frequency, ω/ω_1 , where ω_1 is the undamped resonance frequency. The results in Figure 2.1(b) are for $m_2 / m_1 = 0.10$ and for three different critical damping ratios ($\zeta = c_2 / 2 (k_2 m_2)^{1/2}$) of the absorber of 0, 0.05 and 0.20. When the primary structure is excited at the tuning frequency ($\omega = \omega_1$), perfect control effect is possible with an undamped absorber ($\zeta = 0$). This tuning may be very important practically if the primary structure represents a machine, which is designed to operate constantly at this particular tuning frequency.

One significant consequence of adding a tuned absorber to the primary system is to introduce an additional resonance frequency at a frequency somewhat lower than the original resonance frequency. For $m_2/m_1 = 0.10$, the new resonance is approximately at $\omega = 0.8\omega_1$. The problem now is that as the machine is started from rest, before its steady operating frequency is reached at ω_1 , a resonance has to be traversed at about $0.8\omega_1$. Accelerating to the steady state frequency quickly would certainly alleviate this transient resonance problem. However, in order to provide a quick acceleration, the driver of the primary system should have enough reserve power. The driver would not normally need this reserve power at the steady speed, forcing the design to be a wasteful overdesign in order to avoid the transient resonance.

Including some damping in the tuned absorber reduces the transient resonance amplitudes significantly as shown in Figure 2.1(b) for the cases with ζ of 0.05 and 0.20. The problem this time is that as the transient resonance amplitudes are reduced, the tuning effect is partially lost in the steady state. At the operating frequency, a

damped tuned absorber is worse off than the undamped one depending upon the level of damping in it.

An ideal absorber would be the one with the characteristics of a damped tuned absorber as the first resonance frequency is traversed, and with those of the undamped absorber once the steady state operating frequency is reached. To this effect, an ER fluid is used in this study as the working fluid of a sloshing absorber. The unique feature of this particular fluid, of changing phase between fluid and solid under applied electrical potential, is then employed to manipulate the level of damping in the tuned absorber. Next, a brief description of the sloshing absorber with ER fluid is given first with the suggested configuration for a variable damping tuned absorber. Then, a simple numerical model is discussed to predict performance. Finally, experimental observations are presented to support assertions.

2.2 Sloshing Absorber with an ER Fluid

Sloshing is the low frequency oscillation of a liquid in a container. In most cases, presence of sloshing is detrimental such as in transportation of liquid cargo. Hence, effort is required to suppress sloshing to enhance the integrity of the related application (Hara and Shibata 1987, Hayama and Iwabuchi 1986 and Muto et al., 1988). In contrast to suppression, intentionally induced sloshing of a liquid may be used in a similar fashion to that of a tuned absorber. Instead of a mechanical oscillator, such an absorber utilizes the sloshing of a liquid to provide the required force opposition to achieve the control of a primary structure. The control force is the

fluctuating pressure force on the sides of the container. Earlier work suggested promising designs for an effective sloshing absorber (Anderson et al., 1998).

In a sloshing absorber, energy dissipation is the result of the shearing of the fluid as velocity gradients are developed within the flow. This dissipation increases with the viscosity of the liquid. A schematic representation of a sloshing absorber is shown in Figure 2.2 attached on the same primary structure as in Figure 2.1(a). An ER fluid is used in this study to provide a varying “apparent” viscosity leading to a varying energy dissipation characteristic for a sloshing absorber.

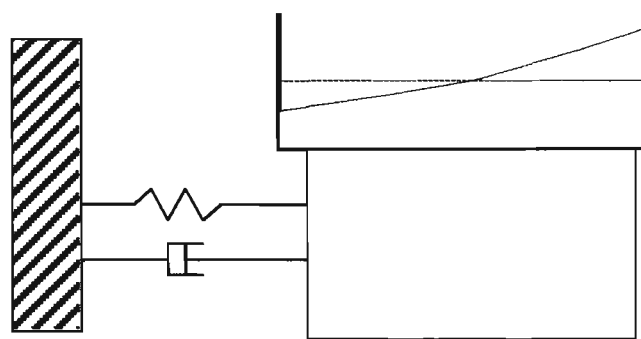


Figure 2.2. Sloshing absorber attached on the primary structure to be controlled.

As mentioned earlier in this section, an ER fluid is suggested as the working fluid of a sloshing absorber to provide variable damping for a tuned absorber. When there is no voltage applied on the fluid, it is free to slosh and dissipate energy. Once the required voltage is applied, the phase of the liquid is transformed to that of a solid. In its transformed phase, it is no longer able to slosh to dissipate energy. The two very different energy dissipation characteristics may, therefore, be used to provide variable damping for the tuned absorber. As the frequency of excitation builds up to the steady state, the ER fluid is allowed to dissipate energy with no voltage applied across it.

Once the steady state is reached, energy dissipation in the liquid can be “switched off” by solidifying the ER fluid. The suggested configuration is shown in Figure 2.3.

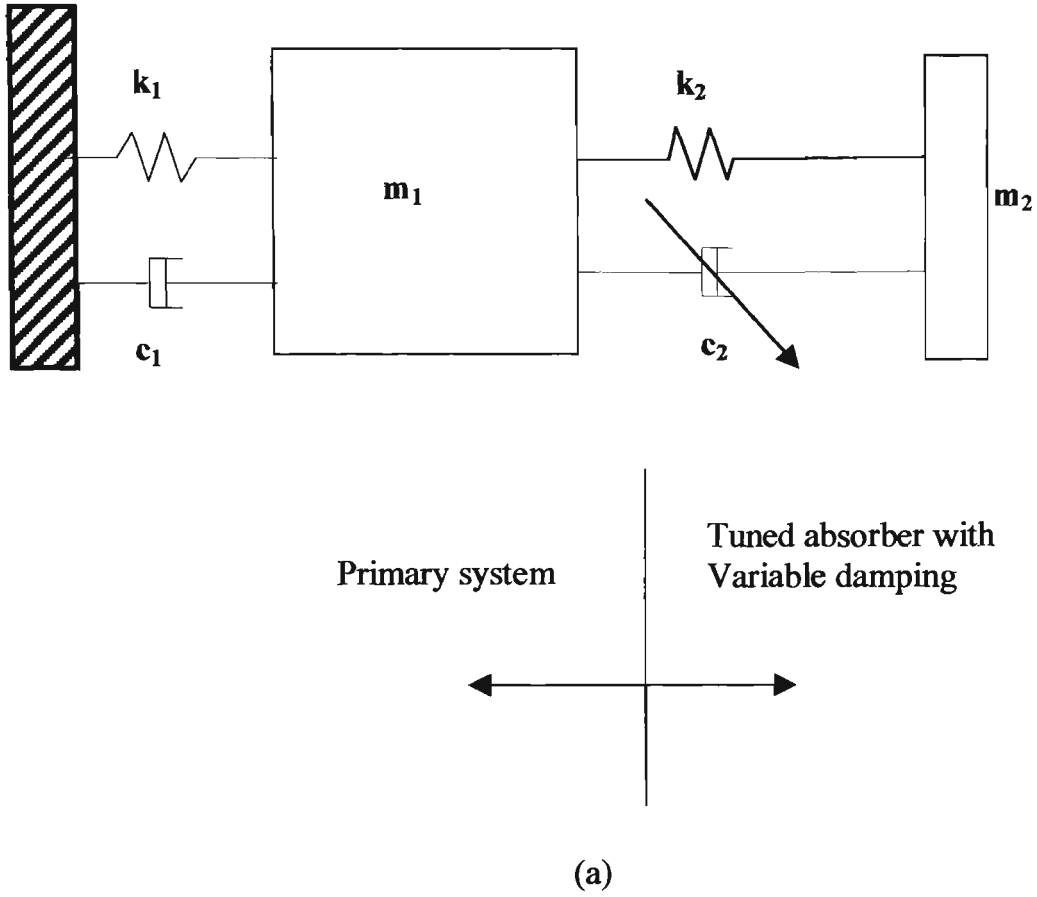


Figure 2.3. (a) Tuned absorber with variable damping.

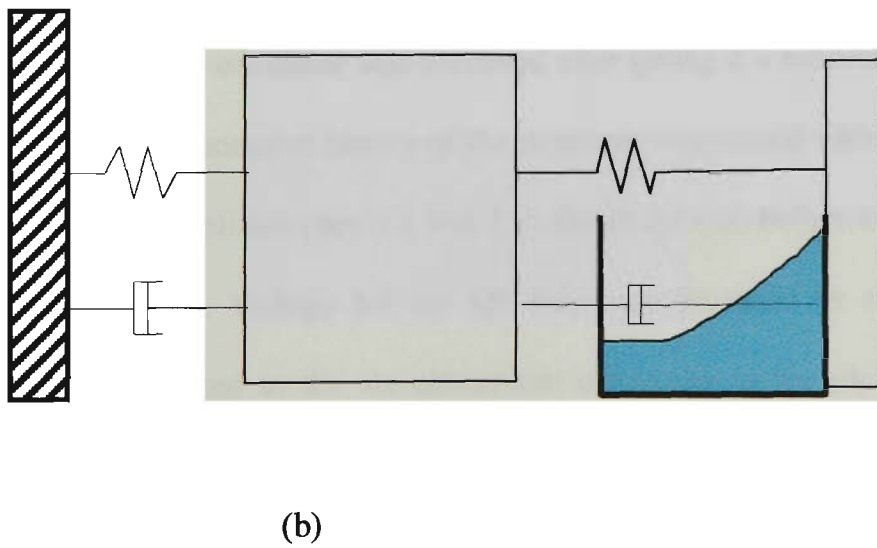


Figure 2.3. (b) Sloshing absorber with ER fluid to provide variable damping.

2.3 Energy Dissipation with Sloshing ER Fluid

A simple experimental setup is shown in Figure 2.4(a) to measure the amount of damping possible with a sloshing ER fluid. The structure consists of a light rigid plate suspended over four thin aluminium strips cantilevered from a fixed base. The container of the sloshing absorber is mounted on the rigid plate. The 100-mm nominal width of a square plastic food storage container is divided into five equal compartments with six aluminium electrodes of 0.5-mm thickness. Hence, 100-mm length of the sloshing wave is maintained for each compartment. Cornstarch, of 40% volume fraction, dissolved in commonly available “light” paraffin oil is used as the ER fluid. An approximately 25-mm depth produced a fundamental sloshing frequency of 2.7 Hz. The fundamental frequency of the structure is also 2.7 Hz when the ER fluid is solidified. This experimental setup is also used as the tuned absorber to control the primary structure to be described in Section 2.5. Structural parameters are summarized in Table 1.

Free decay of the simple oscillator was observed after giving it a predetermined initial displacement. The displacement history of the structure was sensed with a non-contact laser transducer and amplified (items 1 and 2 in figure 2.4 (a)) before it was recorded in a personal computer. Voltage for the ER fluid was provided by a high voltage source (item 4) connected to the six aluminium electrodes in the plastic container. Only two electrodes are shown in the figure for clarity.

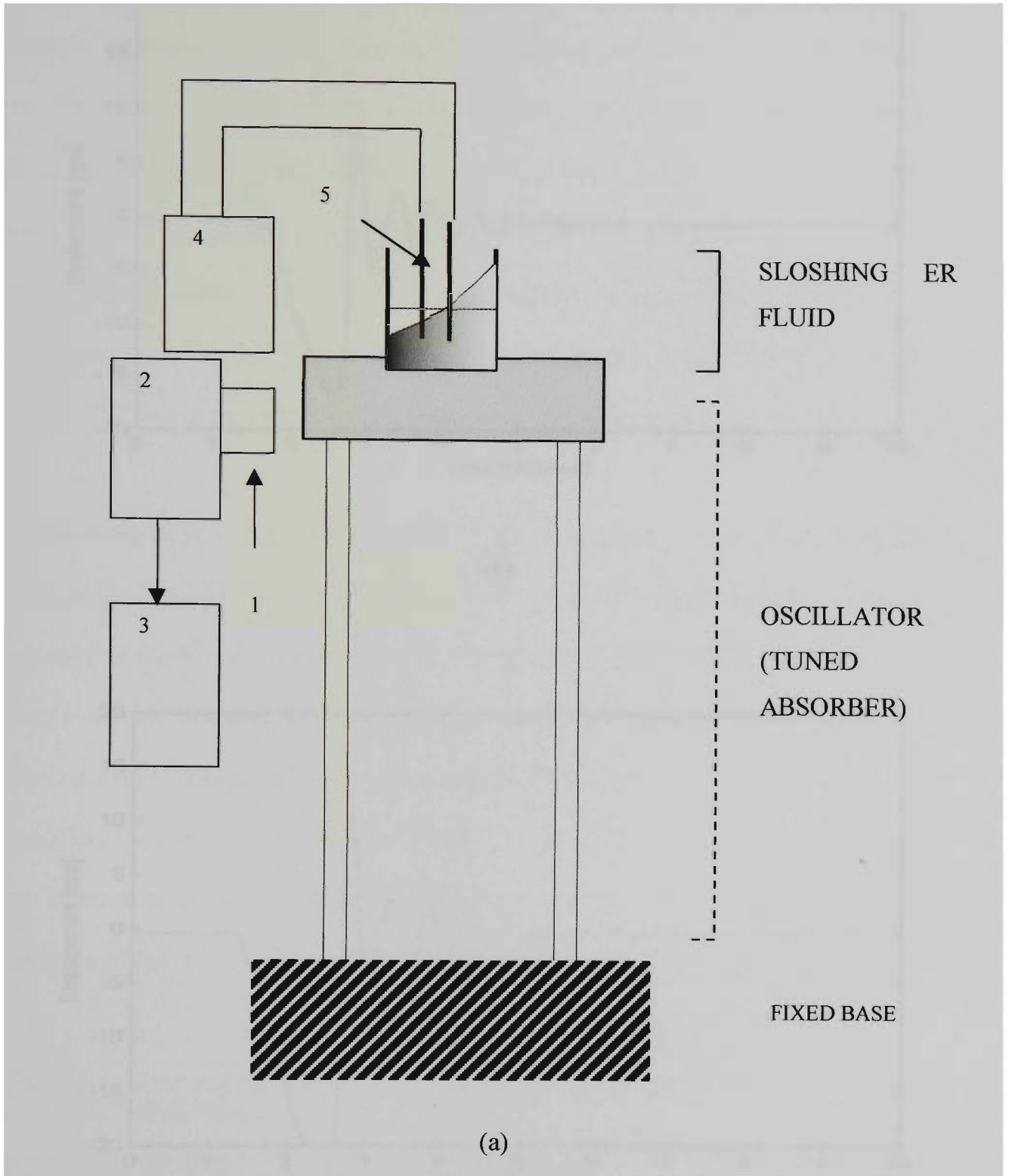
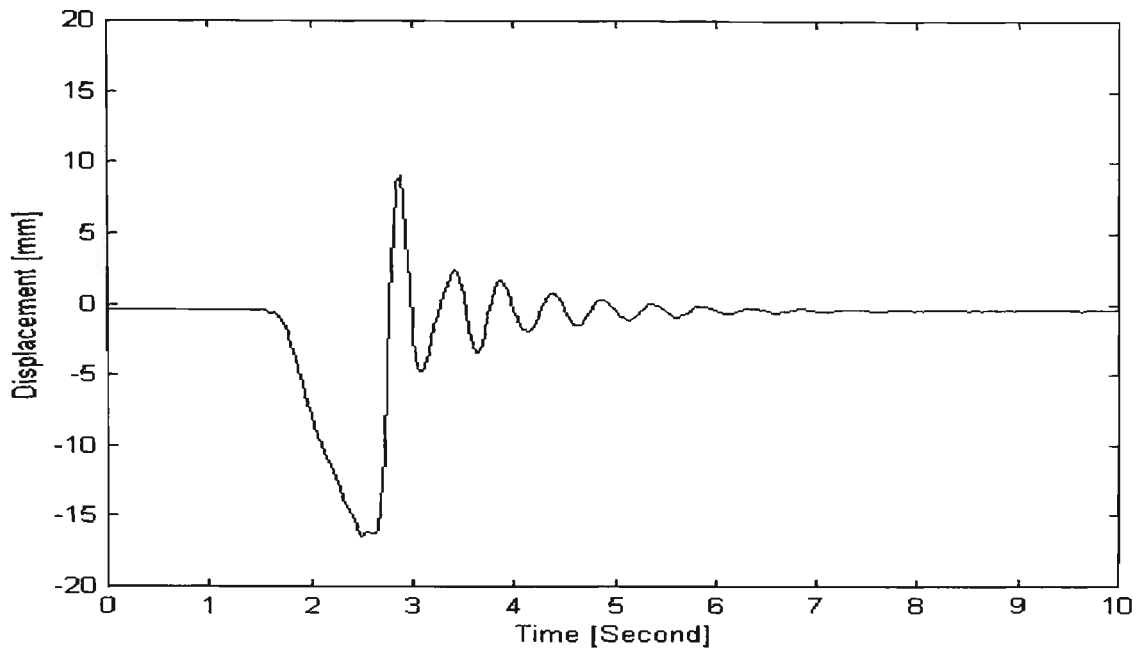
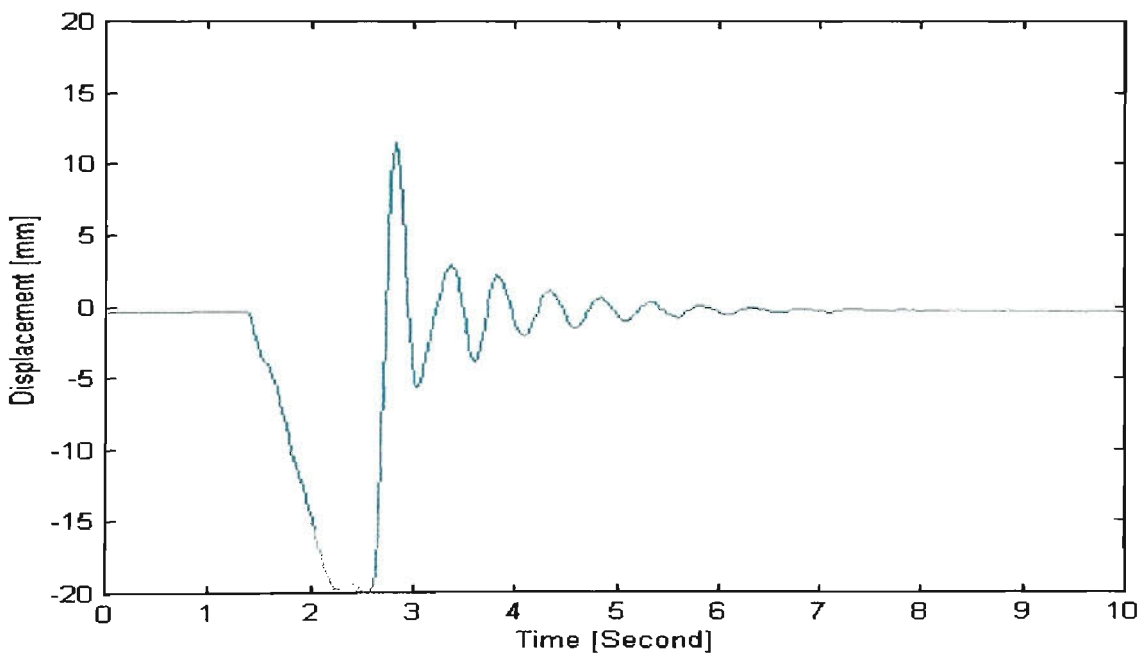


Figure 2.4. (a) Experimental setup

1: KEYENCE LB-12 Laser transducer; 2: KEYENCE LB-72 amplifier; 3: computer with data acquisition and speed controller; 4: FLUKE 408B high voltage source; 5: electrodes (0.5 mm thick aluminium).



(b)



(c)

Figure 2.4. (b) and (c) typical decay histories of the structure with no voltage.

Two typical displacement histories are shown in Figures 2.4(b) and 2.4(c) above. In these figures, the oscillator is released from an initial displacement around 2.6 seconds. Of importance is the time varying characteristics of energy dissipation. At the start, when there is a large amplitude sloshing wave, the equivalent viscous damping coefficient (ζ) could be measured to be as large as 0.20, whereas after about three peaks, the damping ratio assumes a value of about 0.05 and remains approximately constant. This trend is not surprising, considering that sloshing is a nonlinear phenomenon, and a large amplitude sloshing wave imposes a more significant shearing action in the flow than that of a smaller wave.

A maximum of 5kV was possible with the available voltage source which gave 0.25 kV/mm between the electrodes of the container shown in Figure 2.4(a). This electric potential is significantly lower than what is reported in the literature to form strong particle chains. However, the purpose here was to simply prevent sloshing rather than making a high-strength solid-like gel, and 0.25 kV/mm was certainly observed to be sufficient for this purpose. As given in Table 1, damping ratio of the oscillator was measured to be around 0.02 with the full voltage when the ER fluid was solidified to act as an added mass.

Table 2.1. Structural parameters of the experimental setup when each component is tested alone.

	fundamental freq. (± 0.1 Hz)	mass (± 0.01 kg)	equivalent viscous damping ratio
primary structure	3.0	4.00	0.0075 ± 0.0005
sloshing container	2.7	0.30	-
absorber with container	2.7	0.40	0.020 ± 0.005 (at 0.25 kV/mm) 0.20 to 0.05 ± 0.01 (at 0 kV/mm)

2.4. Numerical Prediction

A numerical study was conducted to predict the benefits of varying the damping coefficient of the tuned absorber in Figure 2.1(a) as the frequency of excitation traversed from rest to the tuning frequency. Differential equations of motion for this two degree-of-freedom system are

$$m_1 \ddot{x}_1 + (c_1 + c_2) \dot{x}_1 - c_2 \dot{x}_2 + (k_1 + k_2) x_1 - k_2 x_2 = F(t) \quad (2.1)$$

and

$$m_2 \ddot{x}_2 + c_2 \dot{x}_2 - c_2 \dot{x}_1 + k_2 x_2 - k_2 x_1 = 0 \quad (2.2)$$

In these equations, coordinates $x_1(t)$ and $x_2(t)$ represent the absolute displacement of m_1 and m_2 , respectively. An overdot represents differentiation with respect to time. The numerical procedure consisted of preparing a program within the Matlab (Etter 1993) environment to numerically integrate the coupled equations of motion using a Runge-Kutta scheme. The computer program prepared for this purpose is given in Appendix A.

The external force in Figure 2.1(a) was specified to be “ $F(t) = (C\omega^2) \sin \omega t$ ” to represent a rotating unbalance during start-up of machinery. In Table 1, values of the fundamental natural frequency, mass and the critical damping ratio of the experimental structure are given. These values were measured when each oscillator was tested individually as a single degree-of-freedom system. Structural parameters used in the numerical model (namely, the mass, damping coefficient and the stiffness) were calculated from the values reported in Table 1 for easy comparison with the experimental results described in the next section. The excitation frequency ω was

changed linearly up to the tuning frequency, and then, it was kept constant at this frequency, to represent the acceleration and steady state, respectively. The constant C of the excitation is arbitrary, since the system equations are linear.

The displacement histories of the primary structure in Figures 2.5(a) to 2.5(c) shown below correspond to constant damping ratios of the absorber of 0.02, 0.05 and 0.20 as the frequency of excitation traverses from rest to the tuning frequency (2.7Hz) in 100 seconds. The absorber's damping ratio of 0.02 corresponds to the case when the structure described in Section 2.3 is used as the tuned absorber for the primary structure to be controlled, with full voltage applied across the ER fluid. Damping ratios of 0.05 and 0.20 are the two extreme values observed experimentally with a sloshing ER fluid (no voltage). Figures 2.5(d) and 2.5(e) correspond to the cases where the damping coefficient is kept at either 0.05 or 0.20, respectively, until 100 seconds, and then changed to 0.02. Histories of the displacement of the absorber in Figures 2.6(a) to 2.6(e) correspond to the same cases as in Figure 2.5. In order to fit in the same vertical scale, the displacements in Figures 2.6(a), 2.6(b) and 2.6(d) were divided by 2.5 before plotting.

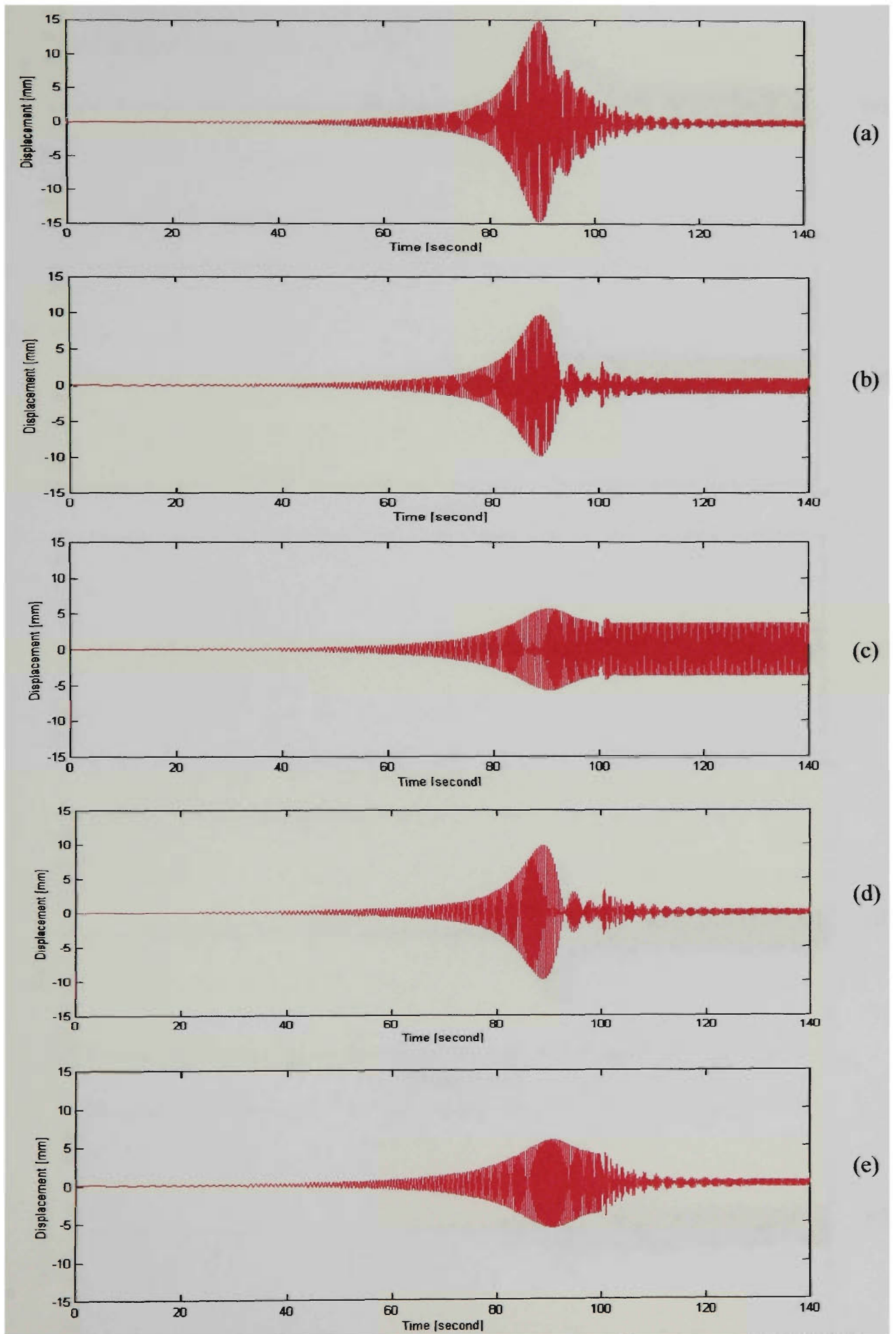


Figure 2.5. Displacement history of the primary structure with a constant ζ of (a) 0.02, (b) 0.05, (c) 0.20; and with a variable ζ of either (d) 0.05 or (e) 0.20 until 100 seconds and 0.02 after 100 seconds.

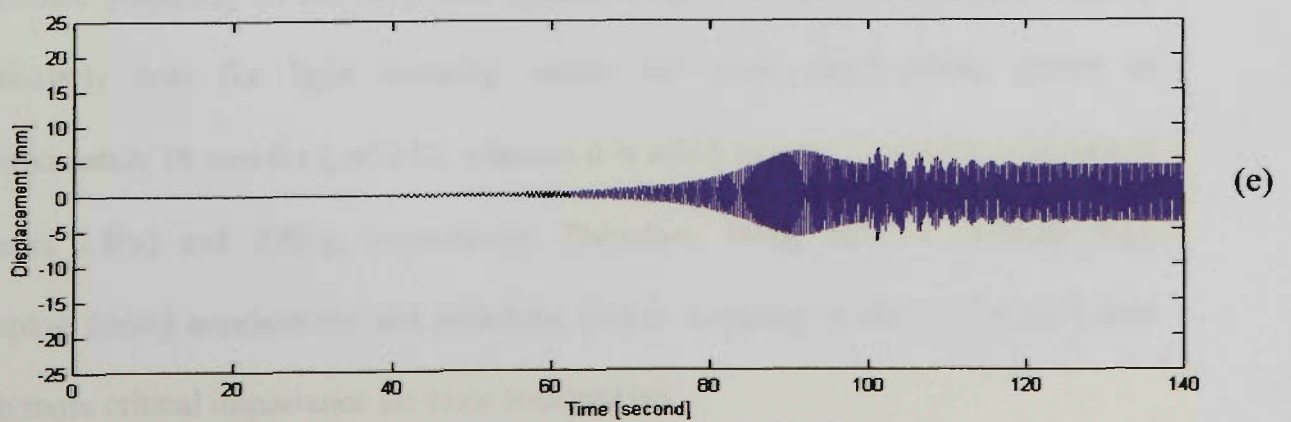
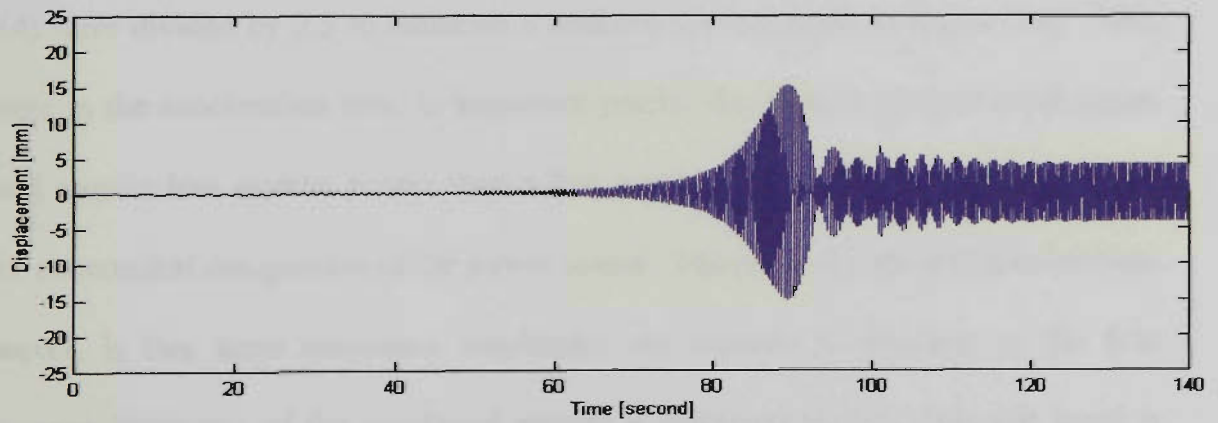
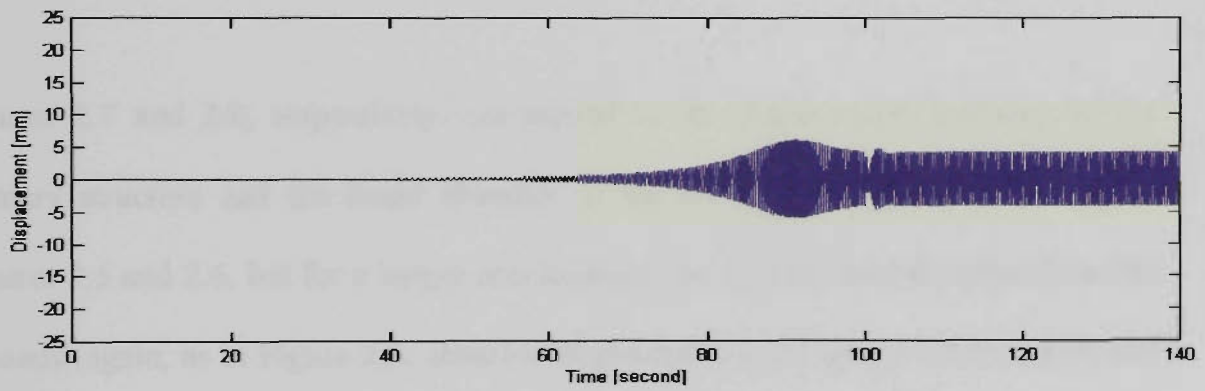
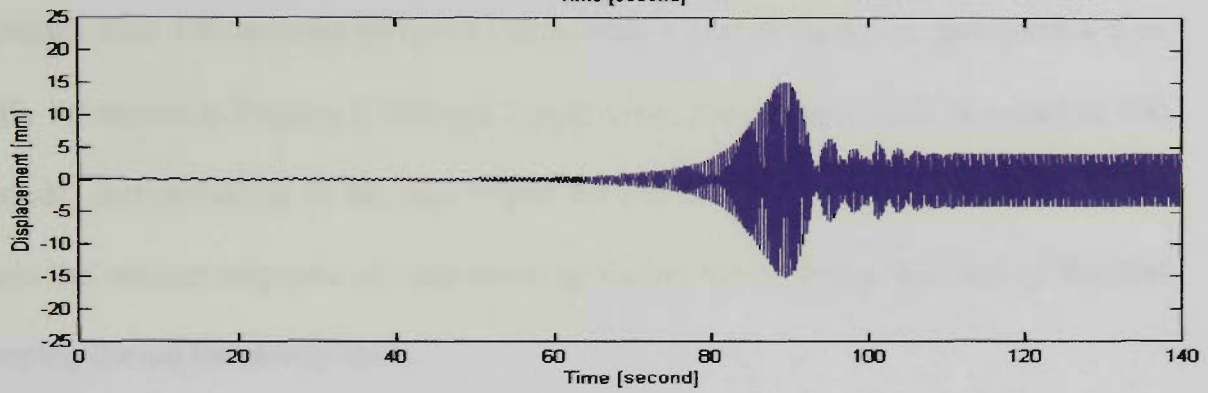
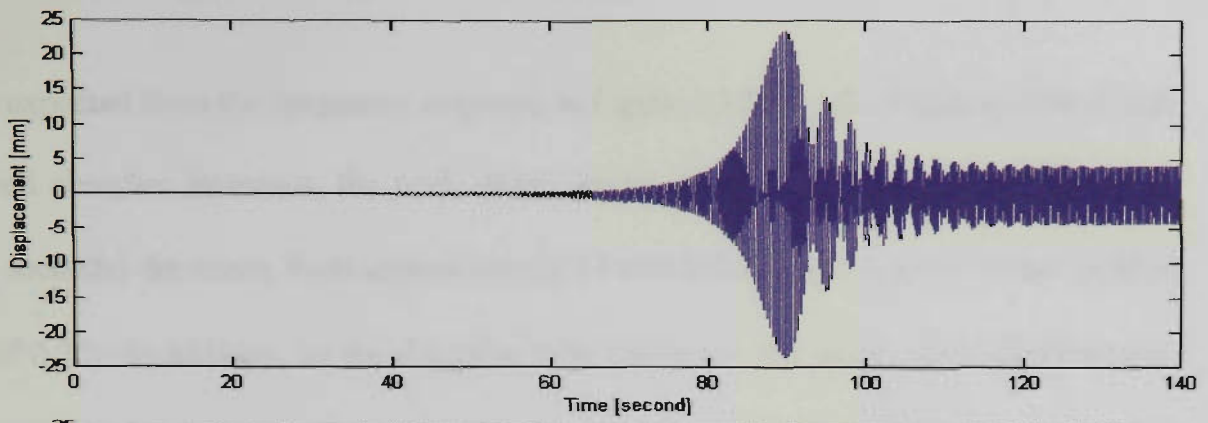
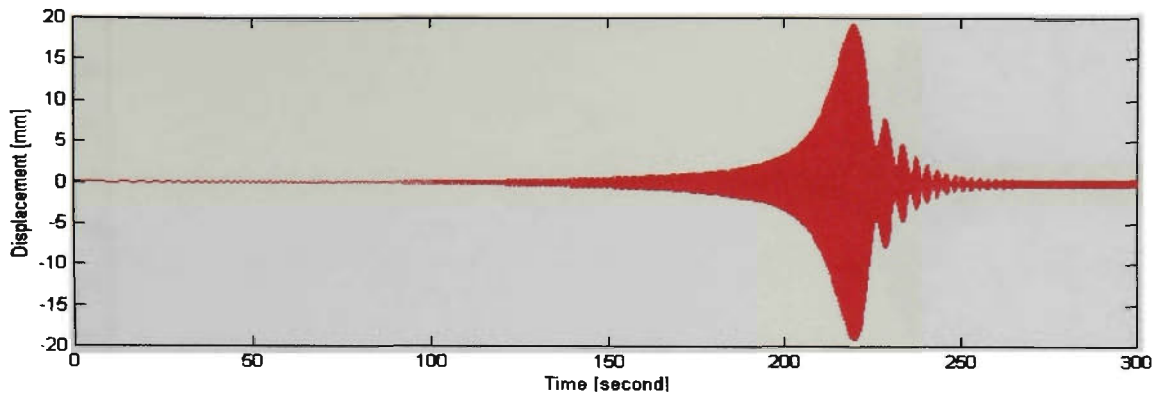


Figure 2.6. Same as in Figure 2.5, but for the tuned absorber.

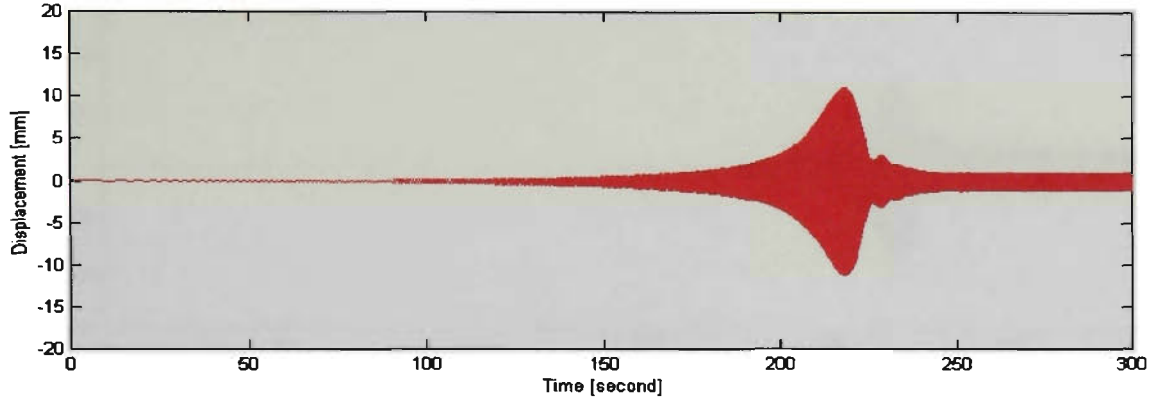
As expected from the frequency response in Figure 2.1(b), as the damping ratio of the tuned absorber increases, the peak displacement during transient resonance (around 84 seconds) decreases from approximately 14 mm (with a ζ of 0.02) to 5 mm (with a ζ of 0.20). In addition, as the damping ratio increases, the steady state displacement increases after 100 seconds from 0.25 mm (with a ζ of 0.02) to 2.6 mm (with a ζ of 0.20). As shown in Figures 2.5(d) and 2.5(e), when the damping ratio is varied at 100 seconds, corresponding to the case where the ER fluid is solidified, it is possible to retain the smaller response of high damping during acceleration, and that of the low damping during the steady state.

Figures 2.7 and 2.8, respectively, correspond to the displacement histories of the primary structure and the tuned absorber of the same damping coefficients as in Figures 2.5 and 2.6, but for a longer acceleration time of 250 seconds rather than 100 seconds (again, as in Figure 2.6, absorber displacements in Figures 2.8(a), 2.8(b) and 2.8(d) were divided by 2.5 to maintain a uniform vertical scale in Figure 2.8). This change in the acceleration time is important practically, since a gradual acceleration would require less reserve power than a fast acceleration, and hence, resulting in a more economical designation of the power source. The price of a gradual acceleration, however, is that large resonance amplitudes are allowed to develop, as the first resonance frequency of the combined system is traversed slowly. This last trend is particularly true for light damping where the peak displacement grows to approximately 18 mm for ζ of 0.02, whereas it is still 5 mm for ζ of 0.20, as shown in Figures 2.8(a) and 2.8(c), respectively. Therefore, being able to maintain high damping during acceleration and switching to low damping in the steady state have even more critical importance for slow acceleration.

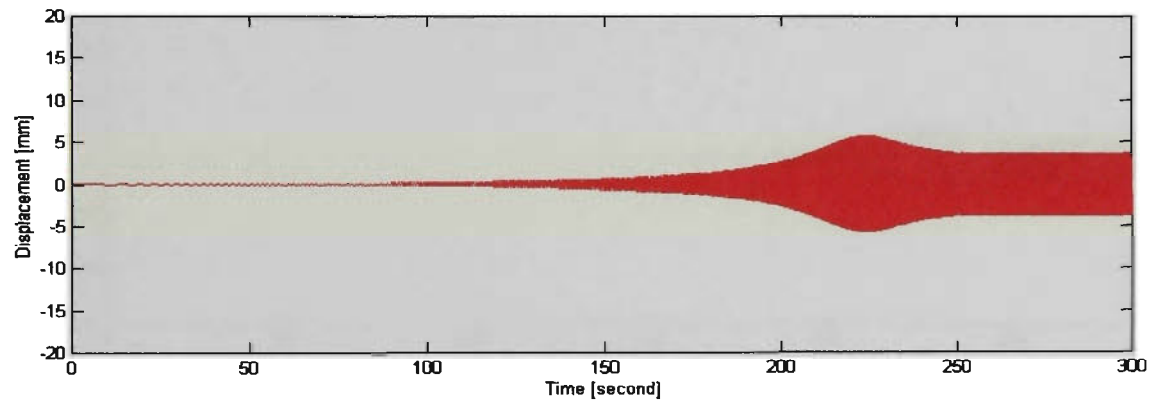
It should be mentioned here that the linear model employed in this section is not claimed to have a true representation of the rather complex energy dissipation characteristics which result from a sloshing liquid. The purpose of including this model is merely to demonstrate the effects of either the existence or the lack of energy dissipation during different phases of the problem.



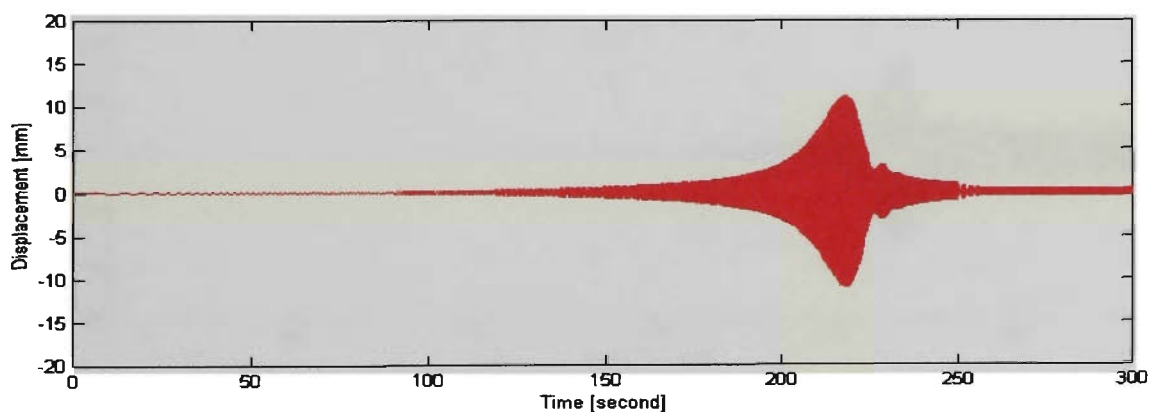
(a)



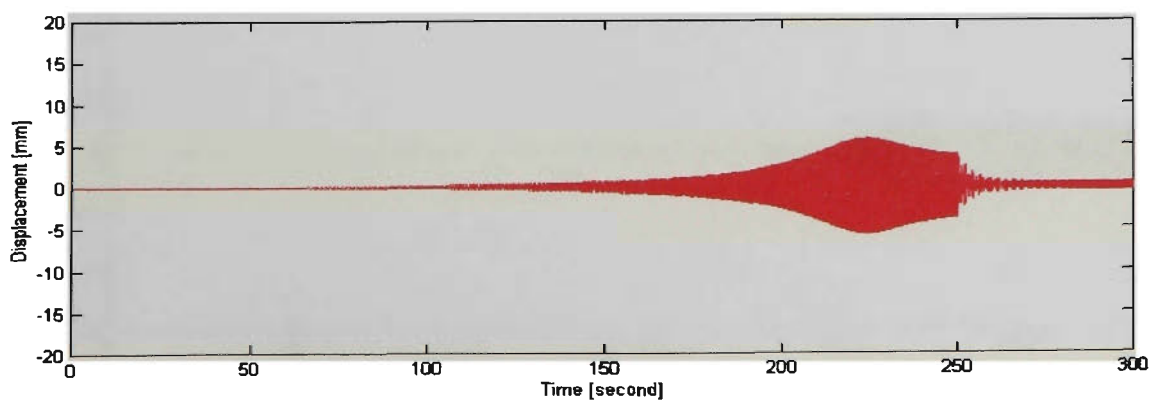
(b)



(c)



(d)



(e)

Figure 2.7. Same as in Figure 2.5, but for an acceleration over 250 seconds.

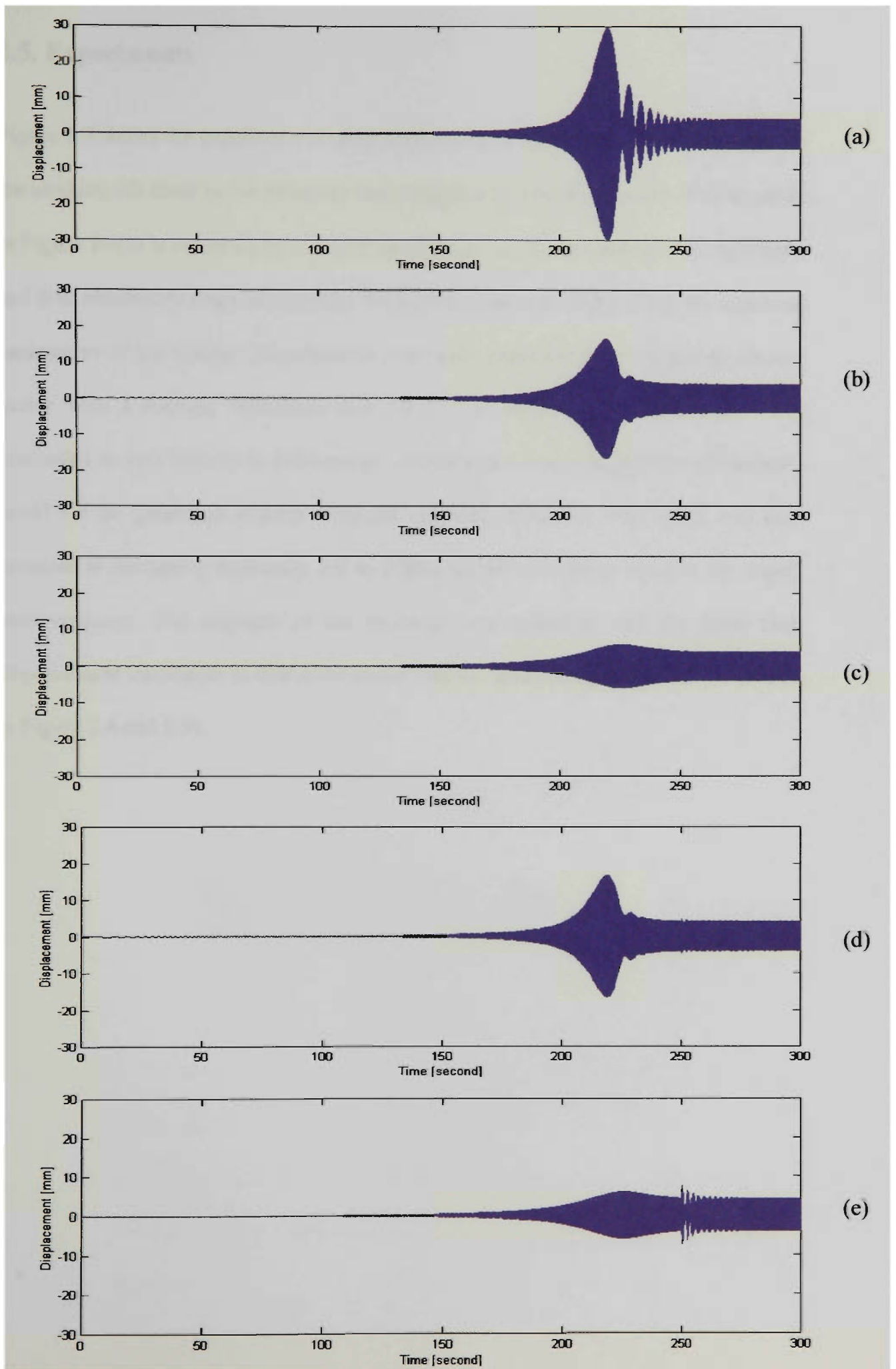


Figure 2.8. Same as in Figure 2.6, but for an acceleration over 250 seconds.

2.5. Experiments

Figure 2.9 shows the experimental setup used to implement the suggested control with the sloshing ER fluid as the means to vary damping of a tuned absorber. The structure in Figure 2.4(a) is mounted on a similar mechanical oscillator made up of a rigid plate and four aluminium strips to represent the primary structure. Table 1 has the structural parameters of the system. Experimental procedure consisted of running a dc electric motor with a rotating unbalance disk (item 6 in Figure 2.9) whose speed was controlled to vary linearly in 100 seconds. Acceleration times longer than 100 seconds could not be generated reliably with the available controller. The speed was kept constant at the tuning frequency for an additional 40 seconds to observe the steady state response. The response of the structure was measured with the same laser displacement transducer as discussed earlier (shown mounted on the primary structure in Figure 2.4 and 2.9).

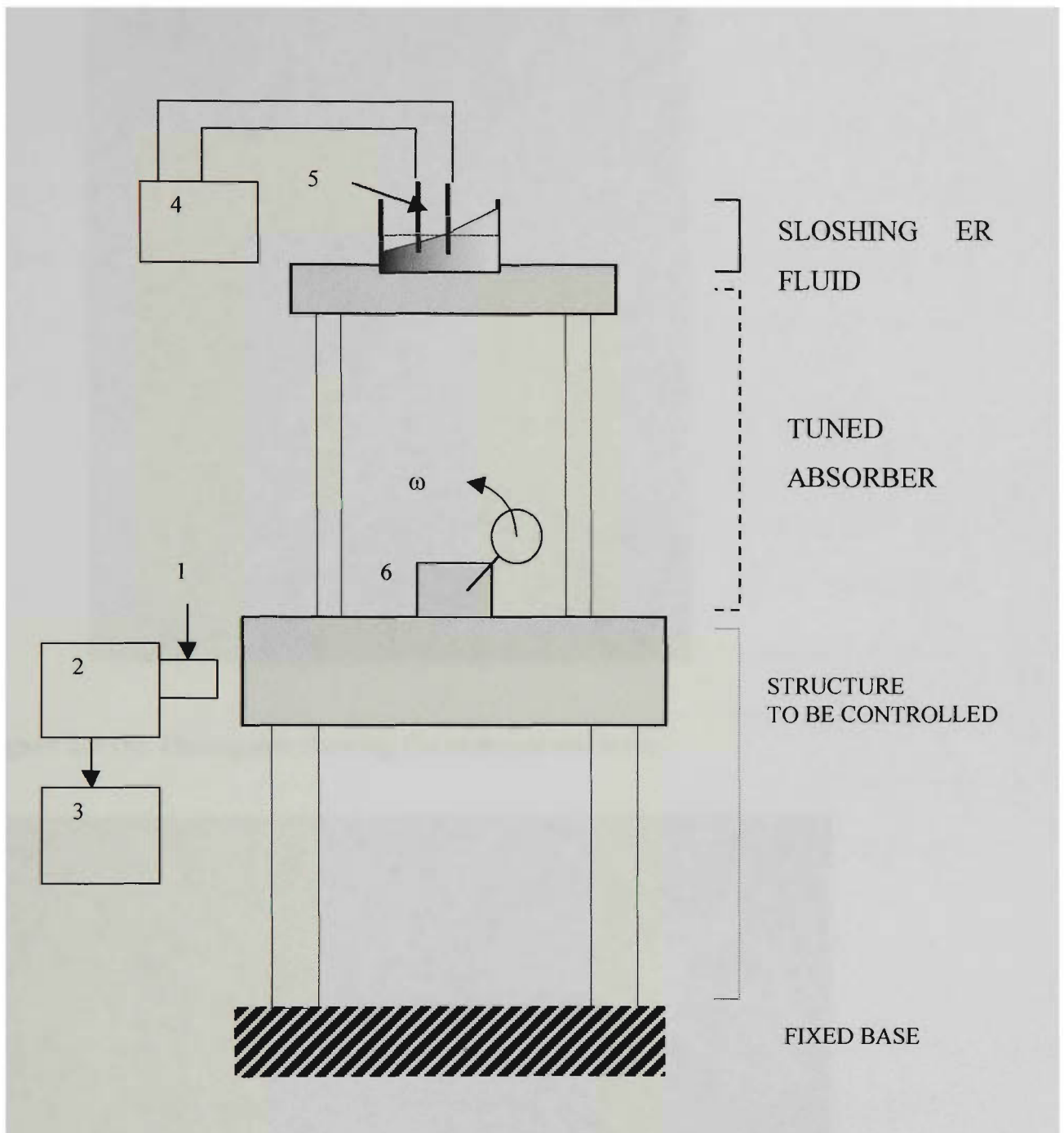


Figure 2.9. (a) Schematic of the experimental setup where the experimental apparatus is the same as in Figure 2.4(a) with the addition of 6: Radio Spares - RS 266-985 dc electric motor with an unbalance disk; and photographs showing (b) the experimental setup and (c) the detail of the sloshing absorber.

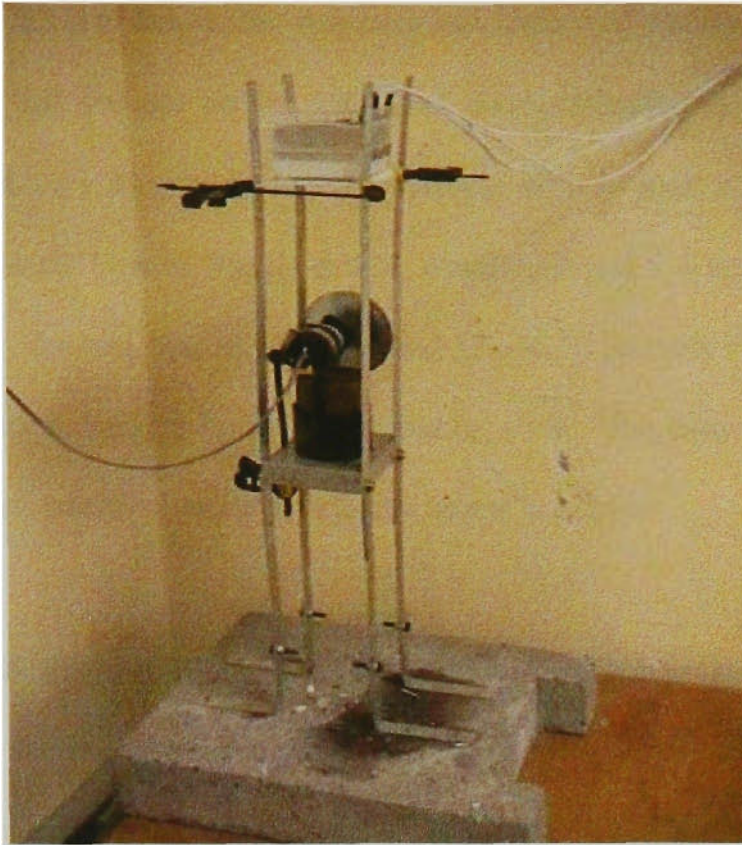


Figure 2.9 (b). Photograph showing the experimental setup.

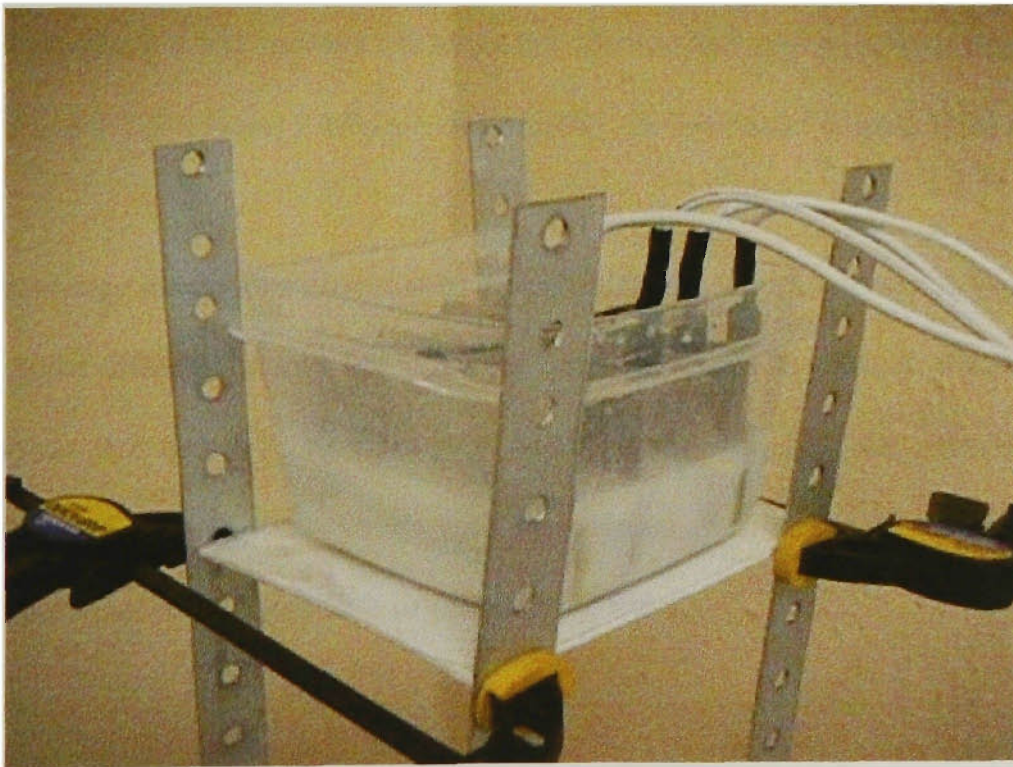


Figure 2.9 (c). Photograph showing the sloshing absorber.

In Figure 2.10(a) below, the displacement history of the primary structure is shown with the full voltage on the ER fluid. This particular case displays the transient resonance very clearly around 90 seconds with a peak displacement response of approximately 11 mm. Steady state is reached around 110 seconds with a 1 mm peak response. The two smaller peaks around 50 and 70 seconds indicate the resonances of the counter balance weights of the rotating disk. The jump change towards the end mark a new transient when the electric motor is stopped.

The displacement history in Figure 2.10(b) corresponds to the freely sloshing ER fluid with no voltage applied on it. As a result of effective dissipation, the transient resonance is virtually nonexistent, whereas the steady state displacement reaches as large as 7mm around 100 seconds. In Figure 2.10(c), the variable damping case is shown where the ER fluid is allowed to slosh freely until 100 seconds, and it is solidified after 100 seconds. As expected, the smaller response parts of the two cases in Figures 2.10(a) and 2.1(b) are successfully combined in Figure 2.10(c).

The energy dissipation provided by the sloshing ER fluid, as shown in Figure 2.10(b), is quite different than what could be predicted with the linear viscous model in Figures 2.5 and 2.7. As discussed earlier in Section 2.3, the amount of energy dissipated with sloshing varies with the amount of shearing in the flow, which is proportional to the amplitude of the sloshing wave.

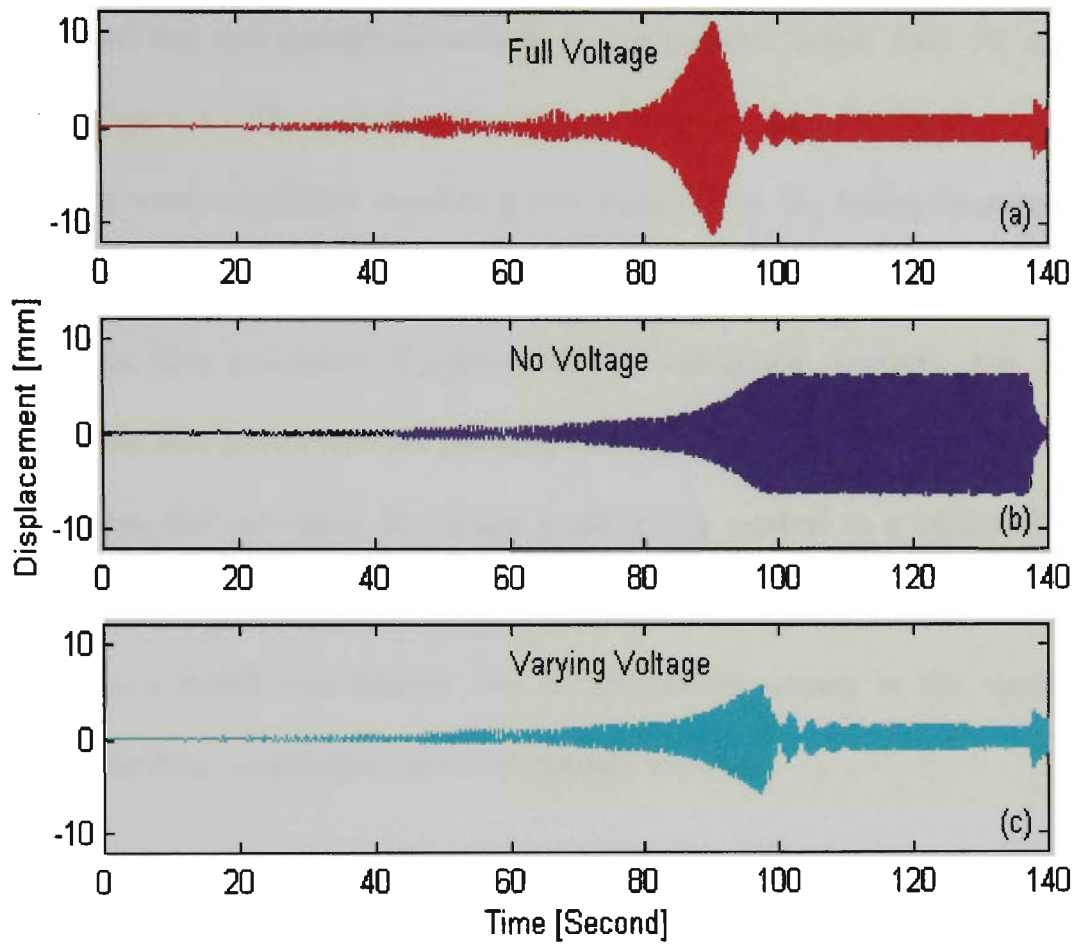


Figure 2.10. Experimentally observed displacement history of the primary structure with (a) full voltage, (b) no voltage and (c) no voltage until 100 seconds and then full voltage.

In Figures 2.11(a) to 2.11(c) below, the displacement history of the absorber is shown for the same three cases as in Figure 2.10. Noise in Figure 2.11(a) is due to the saturation of the non-contact transducer for amplitudes larger than 20 mm. The history in Figure 2.11(b), corresponding to the freely sloshing ER fluid, suggests that the sloshing wave amplitude steadily grows from rest to the tuning frequency. This was verified visually during measurements. As the frequency of the excitation grows close to the first resonance frequency of the combined structure, the effective damping ratio also grows with the growing wave amplitude. With increasing damping in the system, the resonance frequency is constantly pushed to a higher frequency such that the excitation can never catch up with it until the tuning frequency is reached. As a result, the highest rate of dissipation occurs in the steady state producing the large displacements of the primary structure.

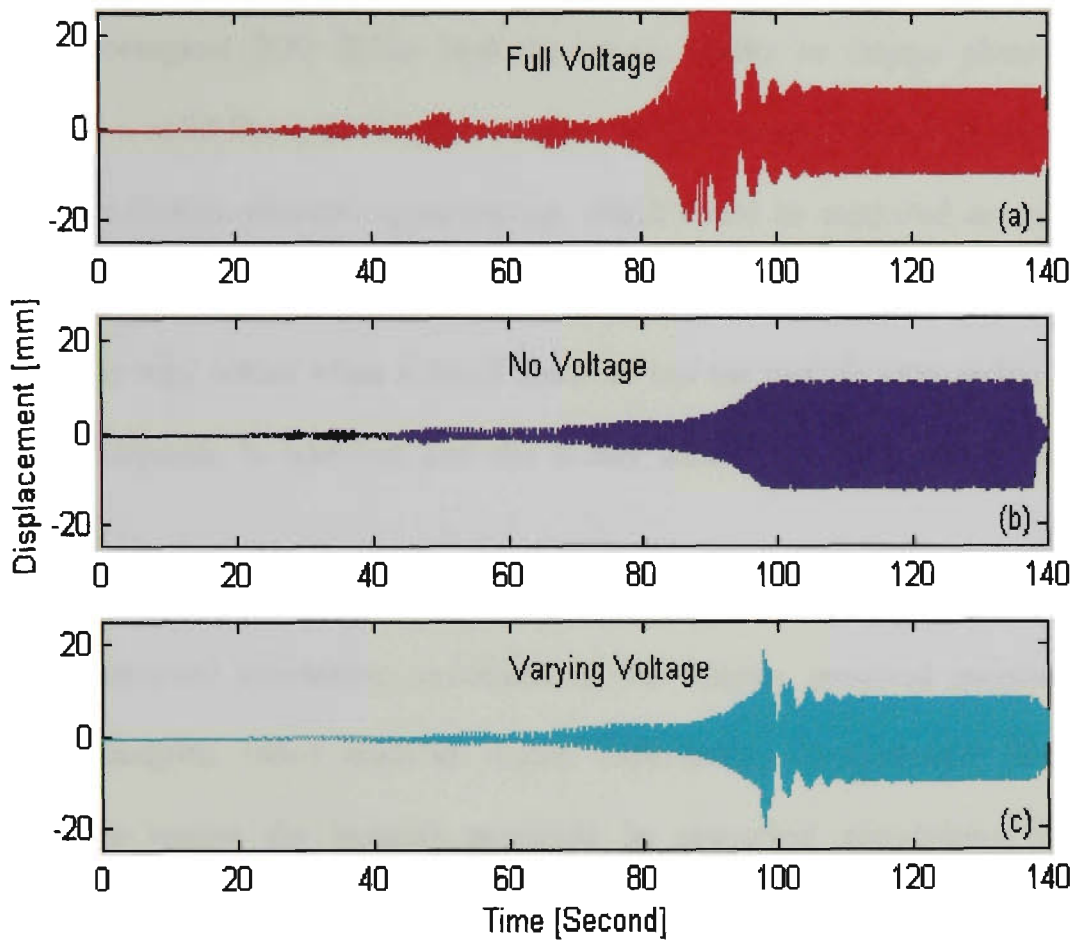


Figure 2.11. Same as in Figure 2.10, but for the tuned absorber.

2.6. Conclusions

Electro-rheological (ER) fluids have the unique ability to change phase between liquid and a solid-like gel with the variation of the electrical potential across them. This phase change presents opportunities, which could be exploited as an agent to switch the dissipation of energy of a tuned vibration absorber. The facility of varying damping is very useful when a tuned absorber has the task of suppressing both the resonant response in transient and the steady state response at the frequency of operation.

Simple numerical simulations presented in this chapter indicated promise of the variable damping tuned absorber. Later, experiments demonstrated that it was possible to realise the benefits predicted by numerical simulations. However, differences occurred between the experimental observations and numerical predictions. It is believed that the differences arose due the fact that sloshing is a nonlinear phenomenon, and this nonlinearity causes the increase in the rate of dissipation with increasing wave amplitude. ER fluids hold potential in applications of vibration control.

Chapter 3

EXPERIMENT DEMONSTRATION OF AN ER CLUTCH

3.1 Introduction

A clutch performs the specific duty of interrupting the transmission of power without shutting off the power source. This is an essential function in many applications such as in road vehicles where changing either intermittent operation of the vehicle in traffic or when the transmission characteristics need to be accommodated with shifting to a different gears.

A conventional clutch operates with the help of friction. The input side of the clutch, where the power source is, operates at the speed of the source. To transmit power, the input and output sides are pressed together engaging the clutch with the help of surfaces lined with high friction material. To disengage, relative motion is allowed between the two sides by gradually releasing them from contact. Before the clutch is disengaged, the two sides have relative motion, transmitting only a part of the input power through frictional forces. After the output loses contact with the input, power transmission is interrupted.

As expected from any friction dependent operation, a conventional clutch suffers from wear. In addition, it is quite likely that undesirable vibrations will be induced in the power train during engaging and disengaging. This chapter proposes is a novel design of a clutch to avoid its inherent problems.

Considering that an ER fluid can change between liquid phase and a solid-like phase in response to electric potential, it may be possible to use it as a power transmission agent with a function similar to that of friction in a conventional clutch. If the function of the clutch is the result of the phase change of the ER fluid, such a design would have no moving components, smooth operation, low power consumption and a fast reaction time.

In the next section, this proposed concept is discussed briefly. Then construction of the prototype model and experimental implementation of the principle of operation are presented. Following the section of the ER fluid clutch, the last section of the chapter discusses a procedure for viscosity measurements.

3.2 Experimental Details

The suggested design for an ER fluid clutch is comprised of two parallel disks with the ER fluid trapped between them. There is no positive contact between the input and output disks. Input power is transmitted to the output disk through the coupling ER fluid. Hence, the suggested design is similar to that of a turbine such that input disk experiences the same speed as that of the power source. The rotation of the input disk causes the coupling fluid to rotate with it at their interface. If the viscosity of the coupling fluid is insufficient to withstand the required shear stress, it will yield and form a velocity gradient between the input and output disks. Considering that increasing electric potential causes an increase in the shear strength of an ER fluid, it may be possible to control the velocity gradient of the ER fluid between the two disks. Maximum value of this gradient is when the output disk is stationary which represents

a disengaged clutch. The minimum value of the velocity gradient is zero, which represents an engaged clutch.

A schematic diagram of the experimental rig is shown in Figure 3.1. Figures 3.2 to 3.5 are the photographs to show different components in detail. In Figure 3.1, a dc electric motor, item 1, is mounted rigidly on a sturdy frame as the input source. The rotational speed of the input source is determined by a dc voltage source, item 2. The motor is connected to drive the top disk (input disk) through a coupler (3) to allow for minor misalignments. The top disk is made of 5mm thick aluminium with a nominal diameter of 121mm. The bottom disk is the output disk. It is hollowed in the form of a cup to retain the ER fluid. When assembled, a nominal gap of 2.5 mm is formed (for the ER fluid) between the two disks. The bottom disk is also made of the same material as the top disk with a smaller 19mm nominal diameter. The output disk is placed on a thrust bearing (item 4) to allow for rotation relative to the frame. A pair of plastic clamps (item 5) is also included; only one is shown in Figure 3.1 for clarity; so that the bottom could be fixed for viscosity measurements.

A second power source (item 6), to provide the required electric potential for the ER fluid, is connected to the disks via coiled phosphor bronze wires forming voltage brushes that provide continuous contact. These voltage brushes are excluded in Figure 3.1, but they are clearly shown in the following photographs in Figures 3.2 and 3.3. Plastic connectors (item 7) are used to electrically isolate the aluminium disks from the rest of the rig.

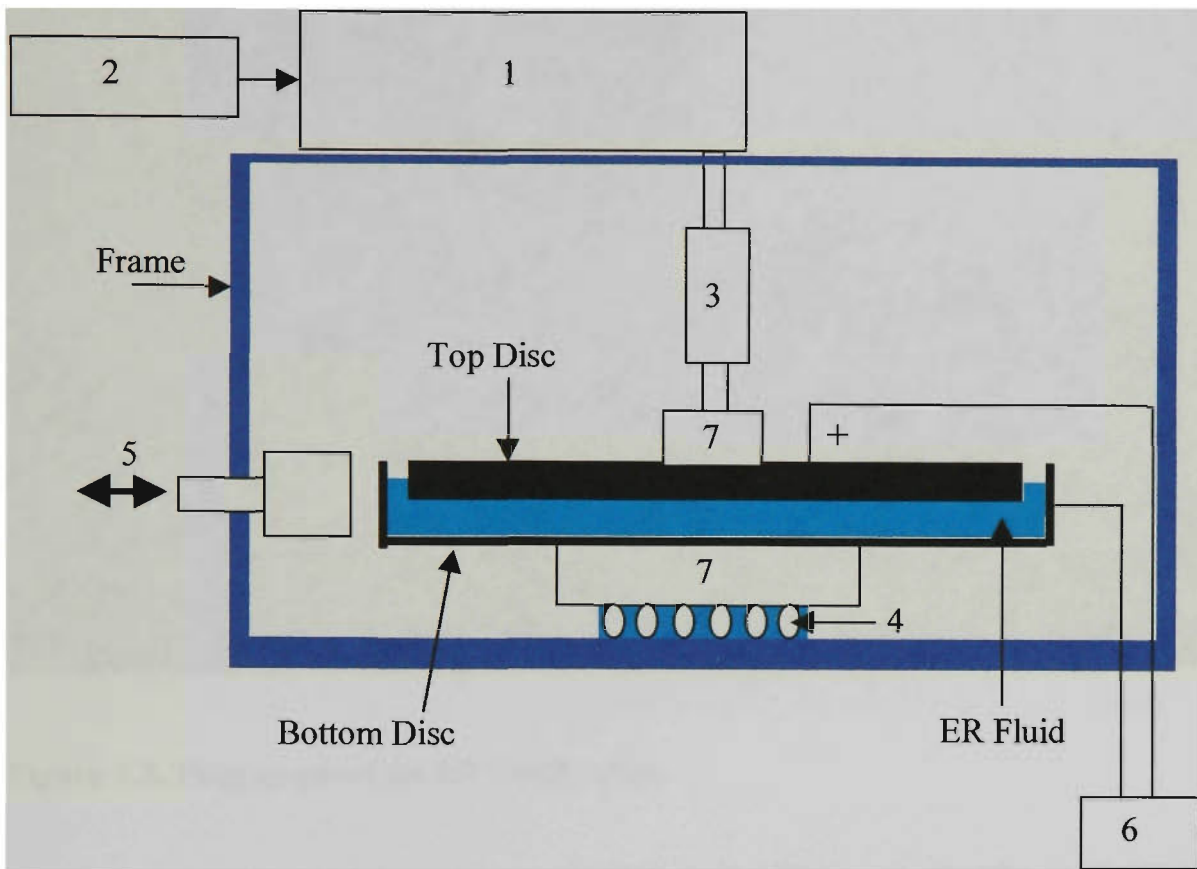


Figure 3.1. Schematic diagram of the experimental setup.

- 1: Any of G2:1-36:1 dc electric motor
- 2: Thurlby Thandar RS 218-835 Voltage source
- 3: Coupling
- 4: Thrust bearing
- 5: Clamp
- 6: Fluke 408B power supply
- 7: Plastic connectors

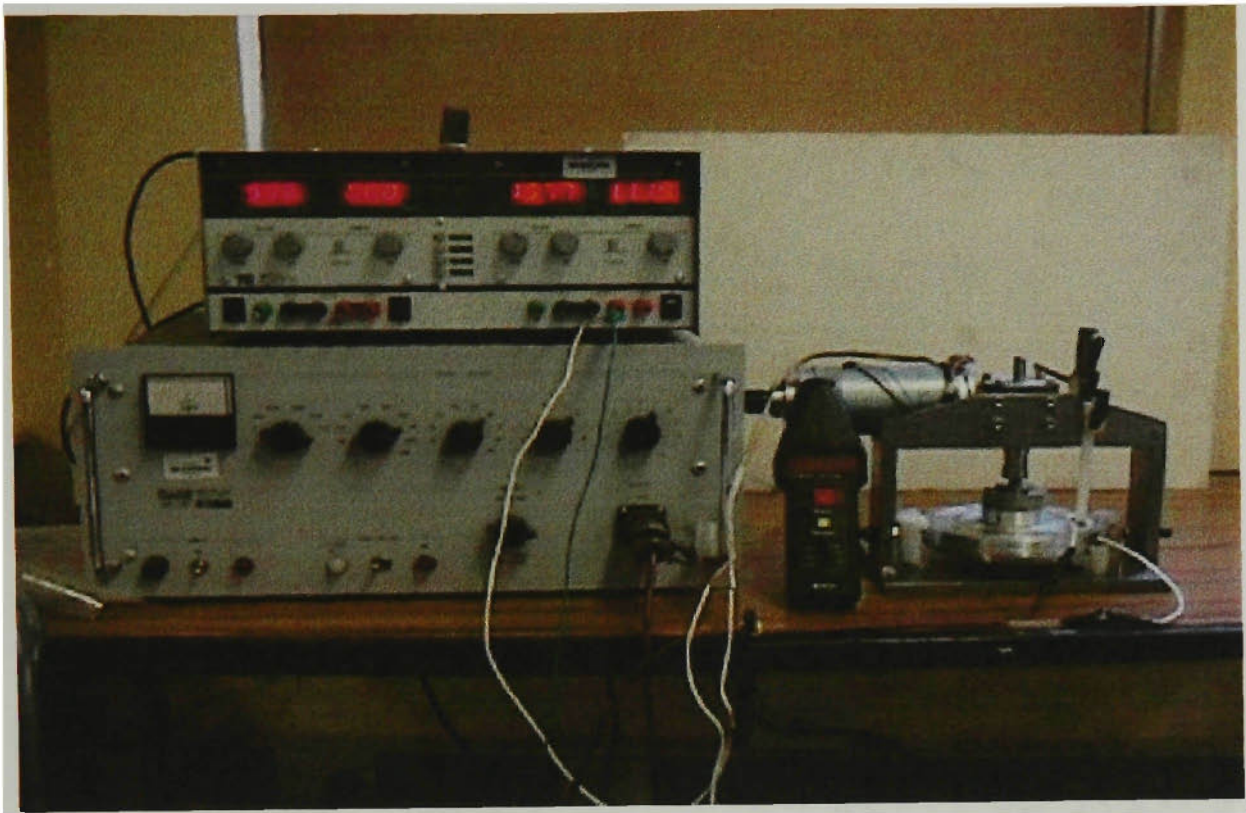


Figure 3.2. Photograph of the ER clutch setup.

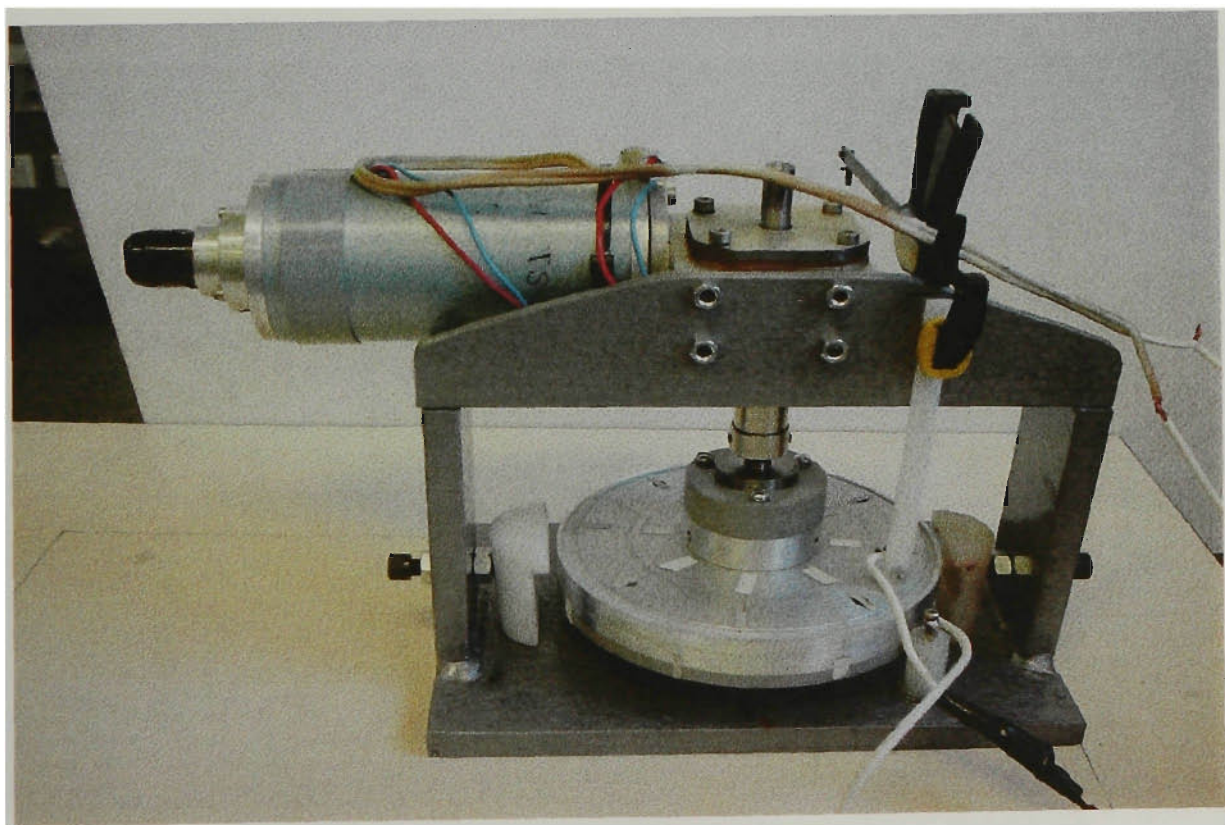


Figure 3.3. Photograph of the ER clutch.

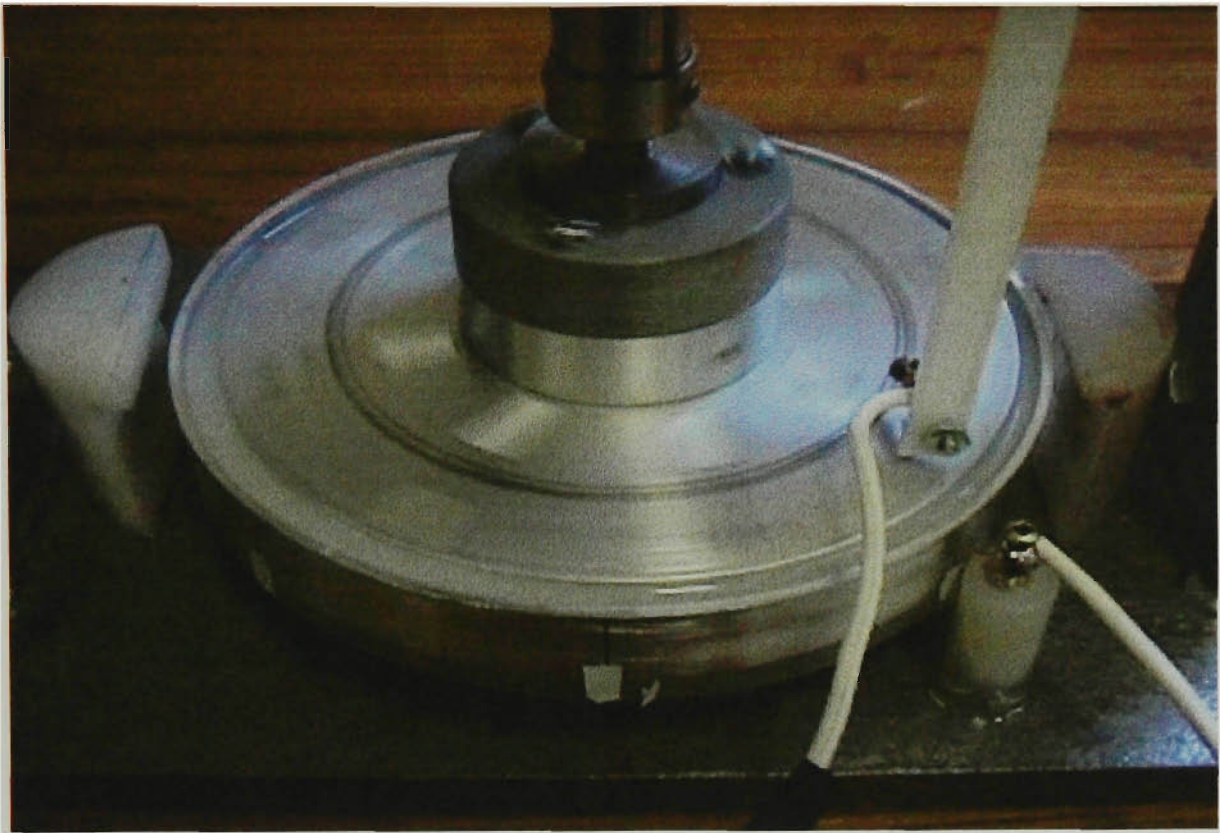


Figure 3.4. Close up of the ER clutch

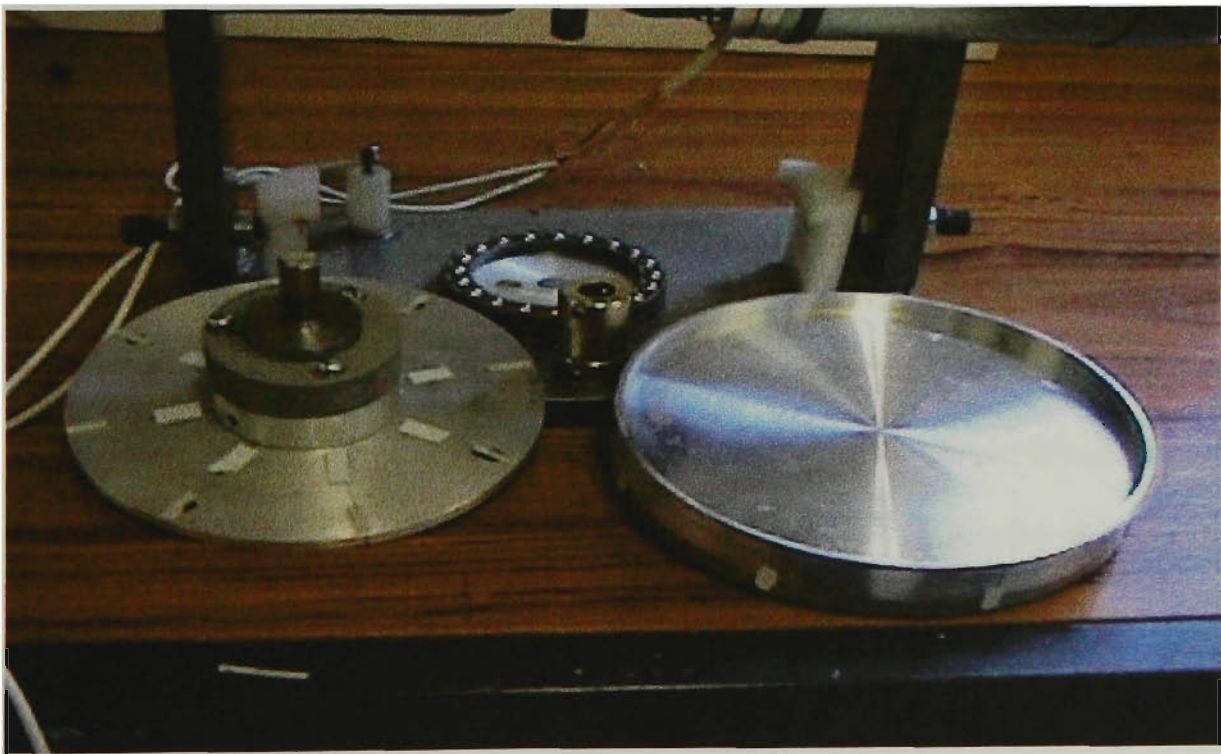


Figure 3.5. A photograph of the ER clutch components.

Experimental procedure included placing the ER fluid with the aid of a graduated syringe in order to avoid spillage. The ER fluid was 40% volume fraction cornstarch in mineral oil. Approximately 45 ml of the fluid filled the 2.5-mm gap between the top and bottom disks. Care was taken to thoroughly stir the ER fluid to avoid settling of the cornstarch. The faces of the two disks were cleaned of any debris in order to avoid arching when the voltage was applied on the ER fluid.

Experiments were performed for input speeds varying between 21 rpm to 73 rpm. For each speed of the electric motor, the speed of the output disk was measured for no voltage on the ER fluid first. This case invariably caused yielding of the ER fluid resulting in lower rotational speeds of the bottom disk than that of the top. Then the voltage was increased with 500V increments until the speed of the output disk matched that of the input disk (at a maximum of 3kV). A hand held tachometer (RS 205-520) was used to measure the rotational speeds with an accuracy of ± 1 rpm.

3.3 Results

The results of the experiments described in Section 3.2 are given in Figure 3.6. In this figure, varying voltage applied across the ER fluid is given along the horizontal axis, whereas the vertical axis represents the ratio of the speed of the output disk to that of the input disk. When the ratio is zero, the clutch is disengaged. When the ratio is one, the clutch is engaged. Any value between zero and one represents a speed differential as a result of shearing (or yielding of) the ER fluid.

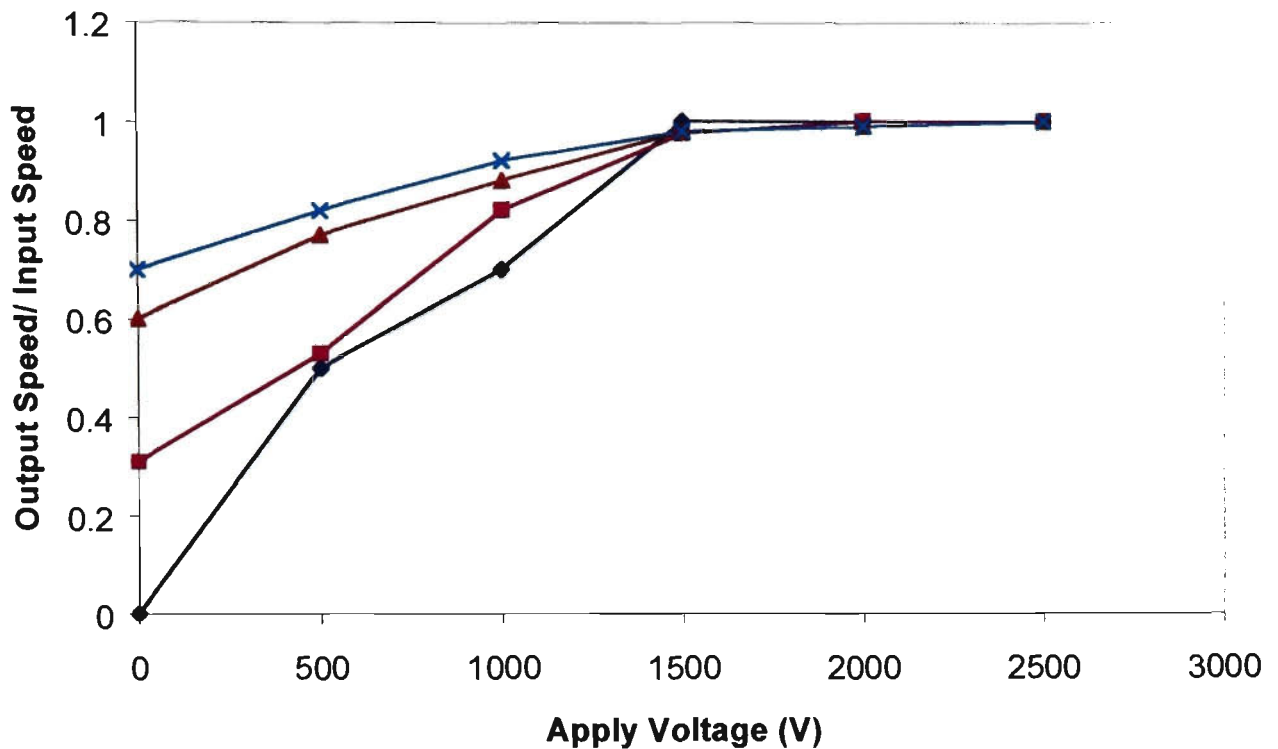


Figure 3.6. Variation of the speed ratio with the applied voltage. ER fluid is 55% volume fraction, cornstarch in mineral oil.

(◆): 21 rpm, (■): 29 rpm, (△): 55 rpm and (✕): 73 rpm.

At the lowest input speed of 21rpm (◆), the output disk remains stationary with no voltage applied across the ER fluid. The fluid shears freely resulting in a disengaged clutch, because of the frictional resistance of the thrust ball bearing. Any increase, starting from 500V, increases the shear strength of the ER fluid and gives a monotonic increase of the speed ratio between the output and input disks until a voltage of 1500V. At 1500 V, the speed of the output disk catches up with that of the input. This voltage gives 0.6 kV/mm across a nominal distance of 2.5 mm between the plates. Any further increase in voltage does not change the speed ratio from one.

At 29 rpm (■), the speed of the input disk creates enough momentum to transfer approximately 30% of the input speed when there is no voltage across the ER fluid. It should be noted that the amount of torque transferred across the clutch is only to overcome the frictional resistance of the thrust ball bearing, between the output disk and the frame of the experimental rig. Hence, a relatively small effort is enough to overcome the bearing friction. However, the trend of the speed ratio is similar to that of the lowest speed where any increase in the voltage produces a monotonic increase in the speed ratio. Again, at 1500V, the speed ratio reaches its maximum value of one. It remains at one for increasing voltages. At input speeds of 55 rpm (▲) and 73 rpm (✕), similar trends to that of 29.3 rpm may be observed with the difference of transferring approximately 60% and 70% of the input speed, respectively, at no voltage.

The results presented in Figure 3.6 clearly prove the viability of an ER fluid clutch concept in principle. It is possible to engage and disengage the output from the input by varying only the voltage across the fluid, without any moving mechanical components in the design. However, it is also recognized that the amount of power transferred across the laboratory prototype is too small to be useful in practice. A bladed assembly similar to that suggested in Figure 3.7 should certainly improve the capacity when output end of the power train has large demands of torque. However, for such a bladed configuration, the power loss and overheating may be exaggerated when the coupling is disengaged. It is also recognized here that the voltage requirements need to be determined for each particular application.

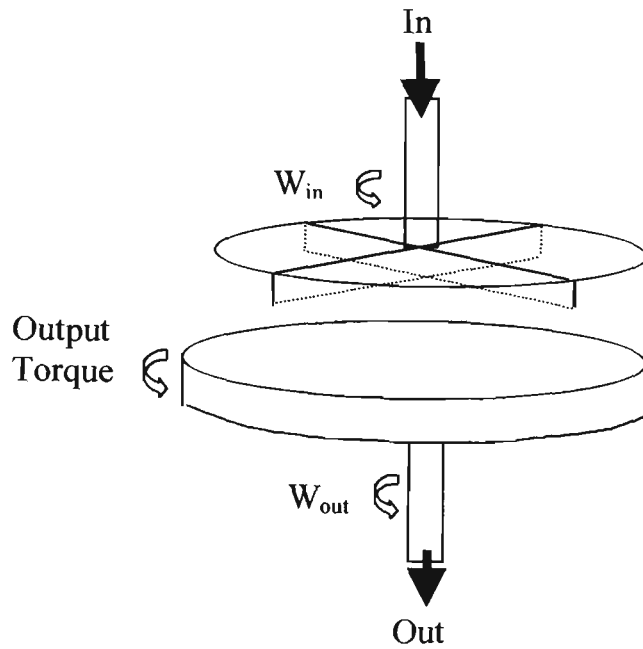


Figure 3.7 Suggested bladed configuration of the input disk to increase the capacity for power transfer.

3.4 Viscosity Measurements

Viscosity of an ER fluid, before any electric potential, and its “apparent viscosity”, with an electric potential, is an important parameter to describe its behaviour. Although the primary purpose of the experimental rig discussed in this chapter was to demonstrate an ER fluid clutch, it was noticed that the same rig may serve double duty by also measuring viscosity. In this section, the necessary equations and the accompanying assumptions are detailed for such measurements.

The test rig has a lock for the bottom disc as shown in Figure 3.1. This feature to keep the bottom disk in a stationary position is needed for viscosity measurements. As a result, the fluid between the two plates is sheared with a velocity gradient resulting from the tangential speed of the top disk and the zero speed of the bottom disk. This

configuration is illustrated in Figure 3.8. In Figure 3.9, the expected linear velocity profile is described schematically between the two disks.

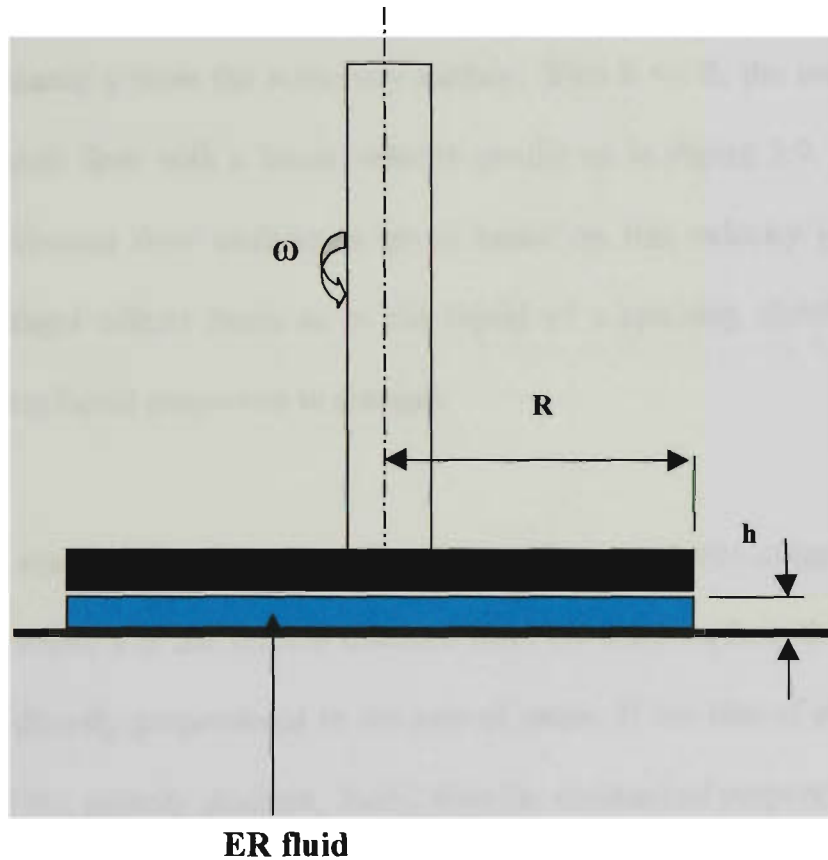


Figure 3.8. Schematic representation of the ER clutch test rig as a viscosity measuring device

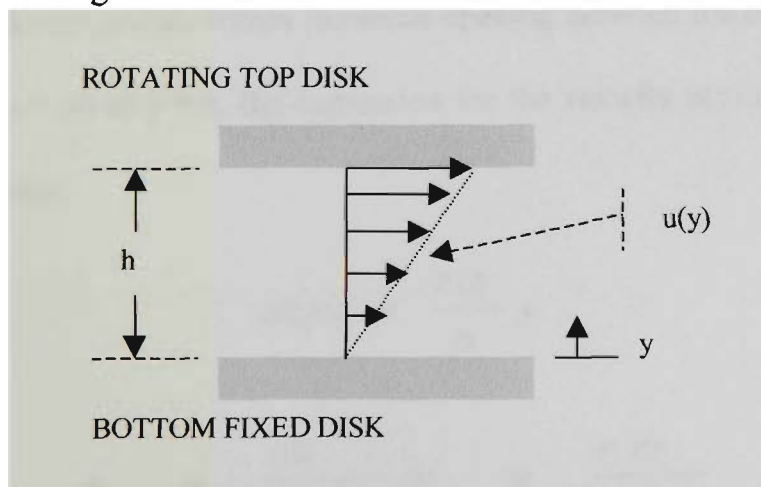


Figure 3.9. The configuration used in the derivation of the viscosity expression.

As indicated in Figure 3.8, the upper plate of radius R of the coupling test rig is to rotate with a constant angular speed ω on a film of ER fluid of small thickness h , such that $h \ll R$. At a radial distance r from the center of rotation, the fluid layer in contact with the moving plate has a velocity $u = r\omega$ and the layer in contact with the lower plate has zero velocity. Intermediate layers have varying velocities, which depend upon their distance y from the stationary surface. With $h \ll R$, the resulting flow is a typical Couette flow with a linear velocity profile as in Figure 3.9. In the following, a simple viscous flow analysis is given based on this velocity profile, excluding any centrifugal effects (such as in the liquid of a spinning clutch) and thermal effects (causing liquid properties to change).

For one-dimensional viscous flow over a solid surface with one velocity component, u , such that $u = u(y)$ where y is the vertical distance from the solid surface, the shear stress in the fluid is directly proportional to the rate of strain. If the rate of strain is expressed in terms of the velocity gradient, du/dy , then the constant of proportionality becomes the fluid viscosity of a Newtonian fluid (White 1994).

With a linear velocity profile within the small opening between the two discs, from $u = 0$ at $y = 0$ to $u = r\omega$ at $y = h$, the expression for the velocity $u(y)$ and the resulting shear stress become,

$$u(y) = \frac{r\omega}{h} y \quad (3.1)$$

$$\tau = \mu \frac{du}{dy} = \mu \frac{r\omega}{h} \quad (3.2)$$

Here, μ is the absolute viscosity of the fluid.

The corresponding shear force causing the fluid layers to deform is

$$dF = \tau dA , \quad (3.3)$$

and the corresponding power is

$$dP = r \omega dF . \quad (3.4)$$

Substituting Equation 3.3 into Equation 3.4,

$$dP = r \omega dF = \omega r \tau dA . \quad (3.5)$$

Thus, the total power on the top disc can be obtained by integrating Equation 3.5 over the entire surface area (for all radii, from zero to R)

$$P = \int_0^R \omega r \tau dA = \int_0^R \omega r \mu \frac{r \omega}{h} 2 \pi r dr \quad (3.6)$$

where the differential area is

$$dA = 2 \pi r dr .$$

After the integration, the corresponding power becomes,

$$P = \mu \omega^2 \frac{2 \pi}{h} \frac{r^4}{4} \Big|_0^R = \mu \frac{\omega^2 \pi}{h} \frac{R^4}{2} \quad (3.7)$$

Rearranging the last power equation for the absolute viscosity

$$\mu = \frac{2 h P}{\omega^2 \pi R^4} \quad [\text{Pa.s}] \quad (3.8)$$

Again, in this last expression, μ is the absolute fluid viscosity [Pa.s]; ω is the angular velocity of the top disc [rad/sec]; h is the fluid height in between the two discs [m]; and R is the radius of the top disc [m]. All the terms on the right-hand-side of the equality can be obtained easily with enough accuracy for the exception of the required power P .

The dc motor to drive the top disk requires a pre-calibrated value of voltage in order to obtain a desired input speed. In addition, the amount of current drawn by the electric motor can be measured. Hence, the required power term in Equation 8 is only possible to measure electrically as a product of voltage and current supplied by the power source.

The inertial resistance of the moving parts and the mechanical loss of the components should remain unchanged for a constant input speed, while the same input voltage is maintained for the motor. Hence, if the two current measurements are collected, one for the top disk spinning freely and the other with the top disk in contact with the ER fluid, the difference between these two measurements should represent the additional effort required to shear the fluid. The product of the current difference and the constant voltage to the dc motor then represents the power term in Equation 3.8, to calculate the viscosity μ .

For a viscosity of $\mu = 2.5$ Pa.s (SAE70 engine oil, at room temperature 20°C, Shigley 1986) and at an input speed of 21 rpm (2.2 rad/s), the required power from Equation 3.7 is approximately 0.16 Watts. Considering that the input voltage is 6V to obtain the required speed, the current differential to shear the fluid is 0.342A. It was impossible to obtain this small a current reading accurately from the voltage source in the

experiment due to the inherent instrument noise. Hence, no viscosity measurements are reported here. It may be noticed that such a noise problem could be overcome by increasing the radius, R , of the disks in the experiment. A five-fold increase in R would result in increase in the power P by 625 times, in Equation 3.7, which is directly reflected in the current differential to be measured.

3.5 Conclusions

In this chapter, an experimental rig is described to demonstrate the working principles of an ER fluid clutch. Such a clutch would have the advantages of being simple in design, having no moving mechanical components, smooth operation and low power consumption. The reported results clearly indicate that there is merit in further investigating this idea.

The suggested clutch rig may also be used for measurement of viscosity. Although the necessary relationships are provided in this chapter, the resulting poor signal to noise ratio prevented collecting reliable measurements with the existing setup. This particular difficulty could be overcome either by using more sensitive instrumentation (lower inherent noise) or by increasing the size of the disks (higher signal). Such efforts were seen to be beyond the scope of this chapter.

Chapter 4

MODIFICATION OF AN AIRFOIL PROFILE USING ER FLUID

4.1. Introduction

The type of operation for which an airplane is intended has an important bearing on airfoil shape selection and wing design. If an airplane wing, including leading edge slats and trailing edge flaps, can be designed to change shape during take-off, cruising and landing, safer flight and higher efficiency of fuel use would be achieved. In this chapter, the objective is to use an ER fluid to provide a variable profile to an airfoil.

During take-off, high lift is required at possibly high angle of attack. Therefore, an airfoil with high lift and low drag characteristics is most suitable for take-off. At cruising speeds, a low drag airfoil is needed to save fuel. When landing, high drag with low lift is required to slow down the airplane. In this chapter, it is attempted to use an ER fluid to switch between different airfoil sections during various stages of flight to obtain an optimal airfoil suitable for a given task. Two airfoil shapes were selected from NACA (National Advisory Committee for Aeronautics) series, NACA0012 and NACA0006, to cover the three stages described above.

NACA airfoils are generated by polynomials describing the shape of the camber line and the thickness distribution. The mean camber line is defined as the midpoint between the upper and lower surfaces, as shown in Figure 4.1. NACA airfoils are described as either a 4-digit airfoil series as NACAxxxx, or a 5-digit airfoil series, as

NACAxxxx. NACA 4-digit airfoil series are based on geometric criteria, with the first digit designating the maximum camber, C_{max} , in percentage chord; the second digit is the chordwise position of the maximum camber, X_{cmax} , in tenths of chord; and the last two digits give the maximum thickness, t , in percentage chord. For example, NACA4412 has a maximum camber of 4% of its chord located at 40% from the leading edge, and its maximum thickness is 12% of its chord. Airfoil numbers starting with 00 have no camber, and they are symmetric. Both NACA0006 and NACA0012 are symmetric sections of 6% and 12% thickness, respectively.

(<http://www.allstar.fiu.edu/wing31.html>).

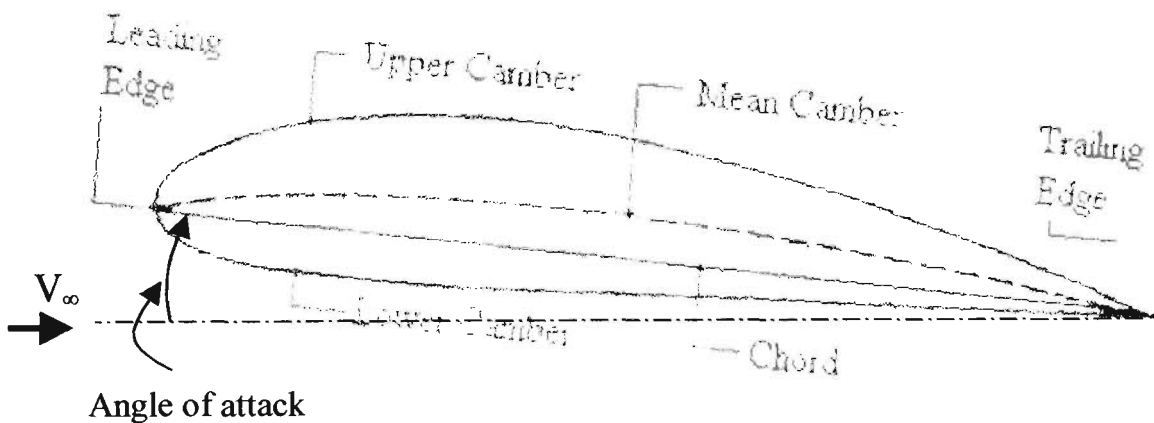


Figure 4.1. Cross-section of an airfoil (from <http://www.allstar.fiu.edu/wing31.html>).

4.2 Aerodynamic Characteristics of a Two-Dimensional Airfoil

The resultant aerodynamic force on a two-dimensional airfoil section can be specified by two components of force perpendicular and parallel to the air stream (the lift and drag forces, respectively) and by a moment in the plane of these two forces (the pitching moment). These aerodynamic loads are functions of the angle of attack of the section, as well as of the Reynolds number, Re . Here, Re is defined in terms of the chord length, c :

$$Re = V_{\infty} c / \nu$$

where V_{∞} is the free stream velocity, and ν is the kinematic viscosity of air, $\nu = \mu / \rho$. Angle of attack is a term used to express the angle between an airfoil's chord and the direction of the relative wind as indicated in Figure 4.1 (Abbott and von Doenhoff 1958).

Lift is the force acting perpendicular to the direction of flight. In level flight, the lift developed by an airplane must be equal to the weight of the airplane. Drag is the aerodynamic force opposing the direction of motion. Drag can be due to surface friction, viscosity (friction drag), pressure distribution caused by the shape of an object (form drag), and lift acting on an finite wing (induced drag) (<http://handleyinnovations.com/glossary.html>).

4.3 Basic Stages of Flight

The flight of an aeroplane may be considered as consisting of various stages: take-off, climb (during which the pilot gains the height at which the level part of the flight will

be made), level flight at a constant height, and finally, glide back to earth and landing (Kermode 1987). These stages of flight are discussed below. The purpose of this section is to clearly identify desirable Lift/Drag characteristics during each of the different stages.

4.3.1 Take-off

As the aeroplane leaves the ground, sufficient lift must be maintained to support the weight of the aeroplane. During the first part of the run, angle of attack is kept small to reduce the drag. When the speed of the aeroplane reaches the minimum speed of flight, the tail is lowered, and the wing is brought to about 15° angle of attack, and the airplane takes-off (Kermode 1987).

4.3.2 Climb

For a normal climb, the thrust force acts in the direction of flight, directly opposite to the drag force. During the climb, the nose is raised to increase the angle of attack. The lift force is therefore momentarily increased, and the aeroplane is accelerated upward until it stabilizes at a steady speed and a steady rate of climb.

The angle of climb depends directly upon the thrust force in excess of the drag force and the component of the weight parallel to the drag force. The larger the weight, the poorer is the climb. Therefore, an aeroplane should generally be kept in a low drag configuration during the climb stage (Kermode 1987).

4.3.3 Level Flight

In steady level flight, the aeroplane is in equilibrium. Lift is equal to weight, and drag is equal to thrust. The lift and weight forces are much larger than the thrust and drag forces, usually by a factor of 10:1. To obtain the required lift at a low speed, a high angle of attack (high lift coefficient) is required, while at a high speed, only a small angle of attack (low lift coefficient) is needed. Figure 4.2 shows Lift/Drag (L/D) versus angle of attack for a general airfoil (Trevor 1996). In this figure, it is shown that L/D increases rapidly up to about 4° angle of attack, where lift is approximately 12 times larger than drag. At angles of attack higher than about 4°, L/D decreases steadily, even though lift still increases for larger angles, drag increases at a greater rate. At the stall angle of attack, L/D is about 5. Therefore, the angle of attack for the best Lift/Drag is approximately 4°. At any other angle of attack, there is a greater cost in terms of increased drag to obtain the same lift.

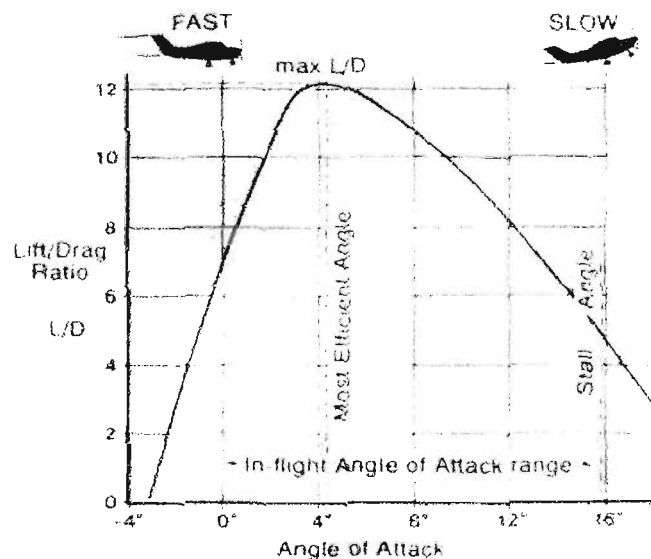


Figure 4.2. Lift/Drag versus angle of attack in general for an airfoil (Trevor 1996).

In steady flight, drag is counteracted by thrust. If the required lift is obtained at the minimum drag cost, then the engine can be smaller, and better economy can be obtained through lower fuel consumption and maintenance cost (Trevor 1996).

4.3.4 Glide and Landing

When an aeroplane is in a steady glide descent, with no thrust being produced by the engine, only three of the four main forces will be acting on the aeroplane, namely, the weight, lift and drag forces. The drag force is no longer opposed with an equal and opposite force, and it will, therefore, act to decelerate the aeroplane. This effect allows the aeroplane to convert potential energy due to its altitude into kinetic energy.

If Lift/Drag is high, the angle of descent is small, and the aeroplane will glide a long way. If Lift/Drag is low, with a lot of drag being produced for the required lift, then the aeroplane will have a large angle of descent.

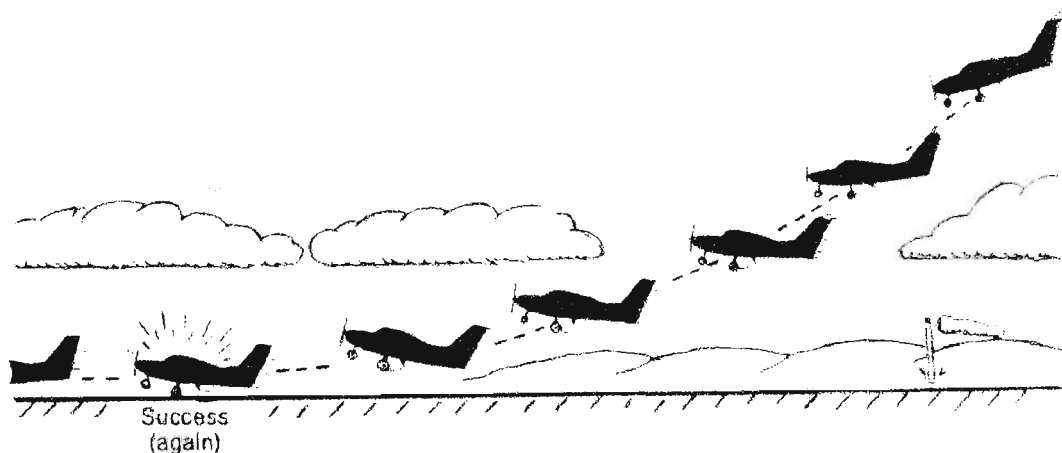


Figure 4.3. Schematic diagram of the landing phase (Trevor 1996).

In the final stage of landing, the engine power is turned off. As the speed is reduced, lift is largely lost. However, the pilot compensates for the decrease in lift through loss of speed by continuously increasing the angle of attack (to approximately 12°) as shown in Figure 4.3 above. When the angle of attack reaches its maximum, lift can no longer be maintained and the aeroplane will settle on the ground (Kermode 1987).

4.4 Aerodynamic Characteristics of NACA0012 and NACA0006

In this section, two standard NACA airfoils are introduced as likely candidates to make a composite airfoil. Such a composite airfoil is able to switch between the two profiles depending upon the particular requirements of different stages of flight outlined previously in Section 4.3.

The two airfoils, NACA0012 and NACA0006, were selected mostly for the suitability of their shapes to make switching between them possible. In addition, NACA0012 has one of the highest lift coefficients (C_L) in the family of symmetrical NACA sections, whereas NACA0006 has one of the lowest. Due their significant differences, they may potentially provide diverse aerodynamic characteristics. The shapes of the two airfoils are shown in Figures 4.4(a) and 4.4(b).

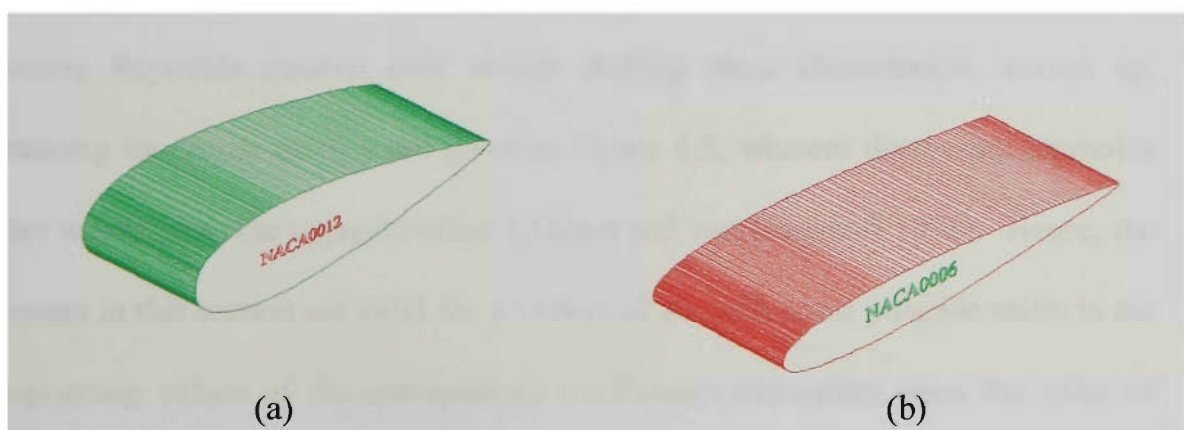


Figure 4.4. Showing the standard profiles of (a) NACA0012 and (b) NACA0006.

Their existing lift coefficient (C_L), drag coefficient (C_D) and pitching moment coefficient (C_M) are given in Figure 4.5 for different angles of attack. Here, these coefficients are defined as follow:

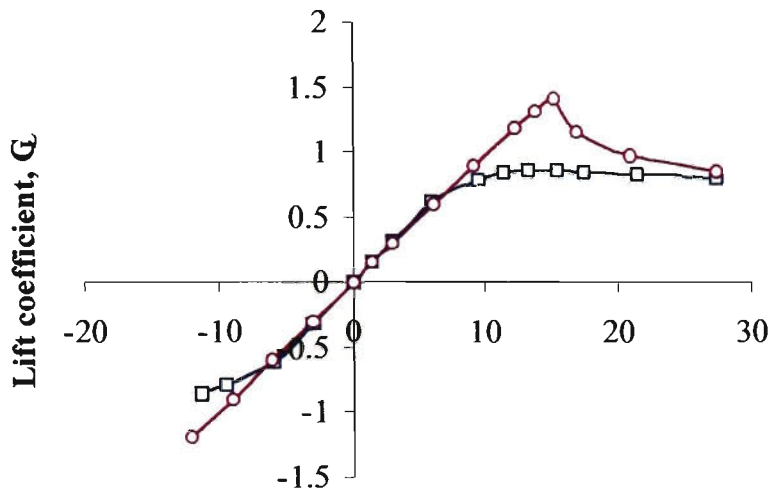
$$C_L = \frac{L}{\frac{1}{2} \rho V_\infty^2 cl},$$

$$C_D = \frac{D}{\frac{1}{2} \rho V_\infty^2 cl},$$

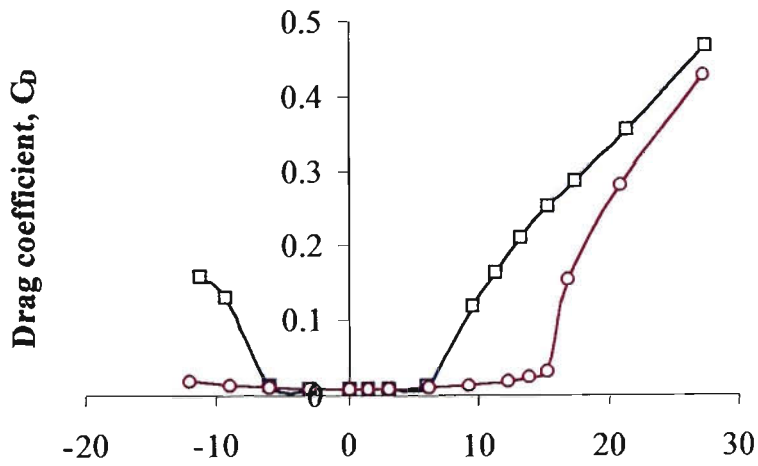
$$C_M = \frac{PM}{\frac{1}{2} \rho V_\infty^2 cl},$$

where c and l are the airfoil chord length and width, respectively. PM is the pitching moment. Large values of these coefficients indicate large values of the lift and drag forces and pitching moment. As a reminder, pitching moment is the moment in the same direction as the angle of attack. Large values of this moment are undesirable, as they would interfere with the intended angles of attack of the airplane.

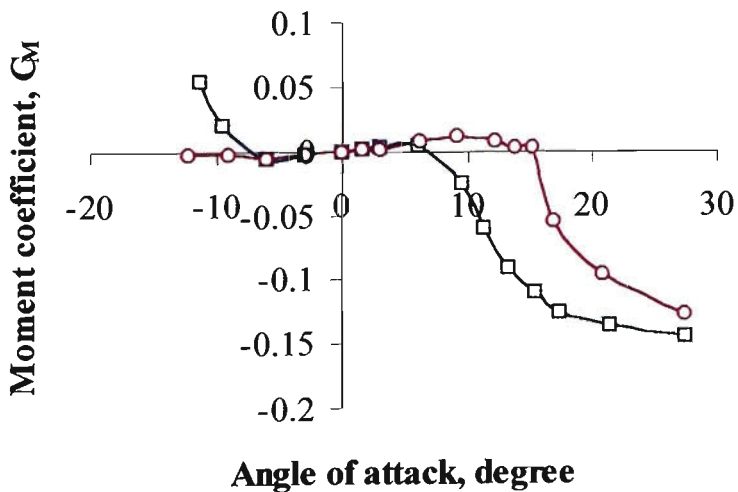
In Figure 4.5, the lift, drag, and moment coefficients are given for only one value of the Reynolds number, of approximately 3,000,000. This Reynolds number corresponds to the minimum speed of a typical airplane in level flight (Jacobs 1931). Increasing Reynolds number only results shifting these characteristic curves up, maintaining the trends as they are given in Figure 4.5, whereas decreasing Reynolds number would have the opposite effect (Abbott and von Doenhoff 1958). Hence, the arguments in this section are valid for a variety of Re with some possible shifts in the corresponding values of the aerodynamic coefficients depending upon the value of Reynolds number.



(a)



(b)



(c)

Figure 4.5. (a) Lift coefficient, (b) Drag coefficient and (c) Pitching moment coefficient of NACA0006 (\square) and NACA0012 (o) (Jacobs 1931).

In Figure 4.5 (a), the maximum lift coefficient of NACA0012 (o) is approximately 1.4 at an angle of attack of 15° (stall angle). Figures 4.5(b) and 4.5(c) show that NACA0012 has a very low drag coefficient of approximately 0.03 and almost zero pitching moment coefficient at the stall angle. Hence, NACA0012 is quite suitable for the take-off and cruising portions of the flight.

The lift coefficient of NACA0006 (\square) in Figure 4.5 (a) is approximately 0.86 at an angle of attack of 15° . In this figure, NACA0006 does not show any sudden loss of C_L corresponding to stall. At an angle of attack of 15° , the drag coefficient of NACA0006 in Figure 4.5 (b) is approximately 0.21 which is seven times larger than that of NACA0012. An increase of angle of attack from 4° to 15° results in a severe increase of the drag coefficient. Also, the pitching moment coefficient increases at high angles of attack as shown in Figure 4.5(c). Hence, NACA0006 is best suited for the landing portion of the flight, because of its low lift, high drag at high angles of attack, and almost zero moment coefficient at low angles of attack. The larger values of the pitching moment may need to be compensated at high angles of attack.

If the two airfoils can be combined together, in such a way that either one of the two shapes can be realised at different portions of the flight, desirable characteristics of each airfoil could be maintained throughout the flight. There are three significant advantageous features of such a combination of the two NACA airfoils. The first feature is to have a short take-off followed by a quick climb due to high lift (of NACA0012). The second feature is low drag at cruising speeds (of NACA 0012). The third feature is a low lift with high drag when landing (of NACA 0006). These features are discussed next.

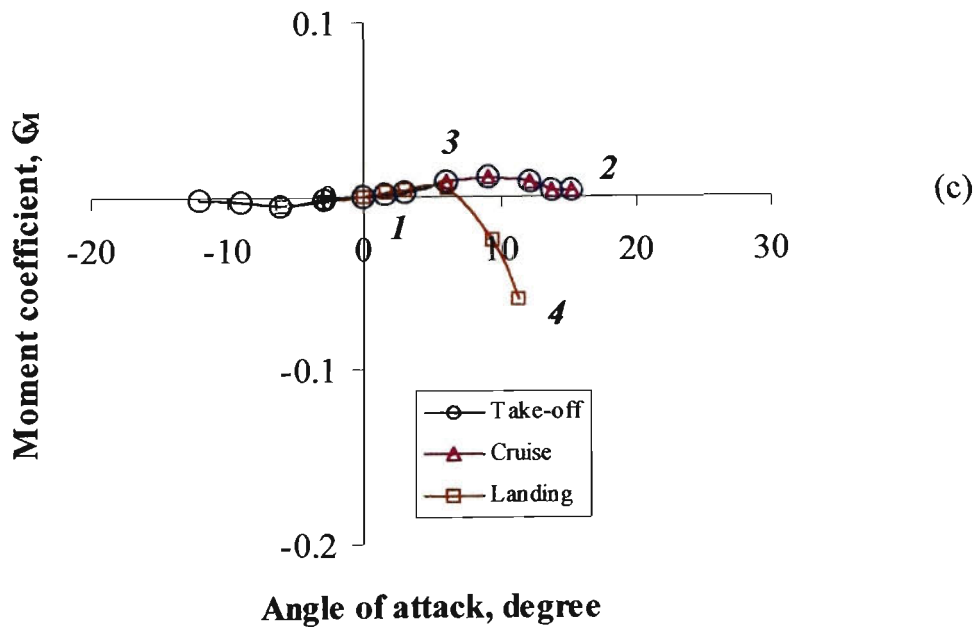
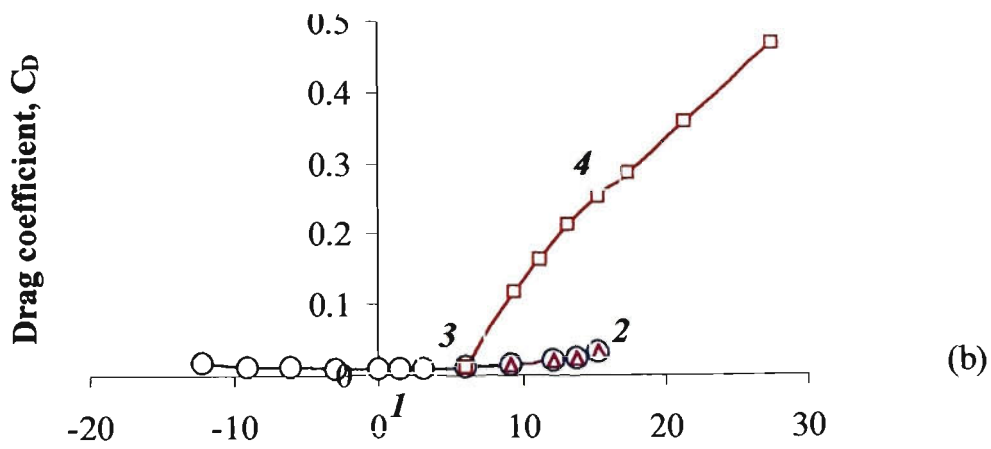
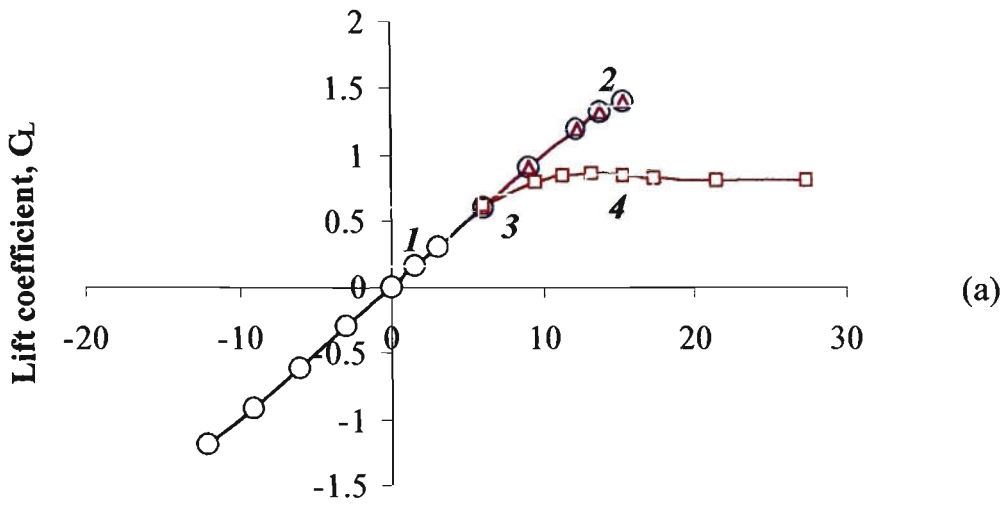


Figure 4.6. (a) Lift coefficient, (b) Drag coefficient and (c) Pitching moment coefficient of the combined airfoil.

During take-off, the composite airfoil starts with the NACA0012 shape to obtain high lift. In Figures 4.6 (a) to (c), take-off is marked from (1) to (2). During cruise, the angle of attack is reduced from 15° to 4° , from (2) to (3) in Figure 4.6(b), to obtain maximum L/D as discussed above. For landing, the composite airfoil is switched from NACA0012 to NACA0006 to obtain high drag to slow down and low lift to lose altitude. Landing is from (3) to (4). In the next section, a laboratory prototype is described to implement the composite airfoil.

4.5 Laboratory Prototype

The purpose of this section is to describe an attempt to accomplish a composite airfoil which can switch between NACA 0006 and NACA 0012. These two airfoils were described in the previous section.

The suggested setup to switch the airfoil shapes is shown in Figure 4.7. In this figure, the airfoil model is shown at the top. Connected to the middle section of the model is a line which transfers the ER fluid to and from the airfoil. A plastic hose of 12 mm outside and 8 mm inside diameter is used for this purpose. In addition, leads are provided to conductor plates from a high voltage source (item 1) to solidify the ER fluid when required. ER fluid is supplied to the middle section of the airfoil from a reservoir (item 2) using a pump (item 3) and valve (item 4). ER fluid is drained back into its reservoir by reversing the direction of the valve, when it is not needed. The design of the airfoil is described next.

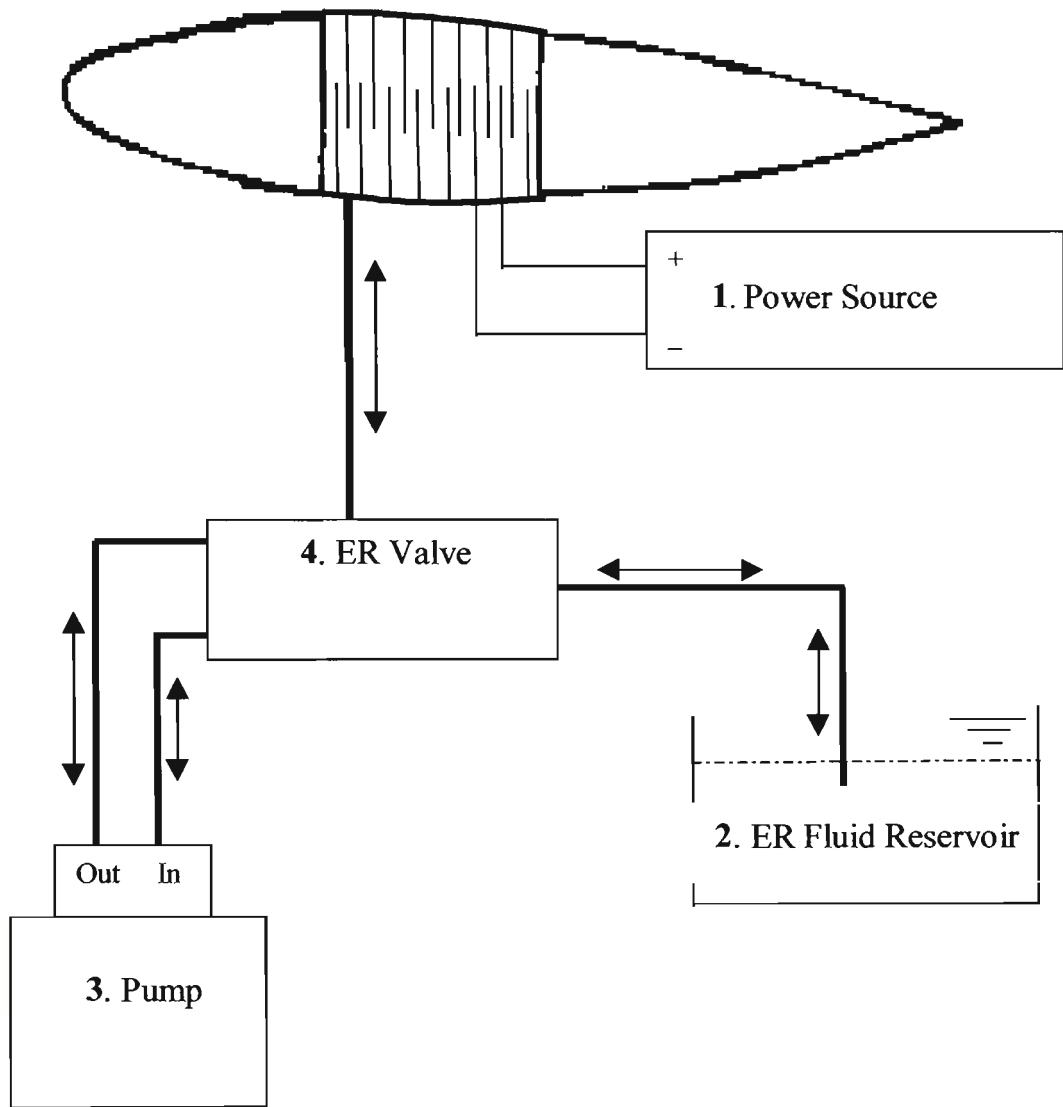


Figure 4.7. Schematic diagram of the overall experimental setup.

1: Fluke 408, Power source, serial no.1912;

2: Reservoir

3: Flojet Pump, FLT 2100-231 MPV, 230 Volt STO ICAM 60 SW, serial no.

94417387;

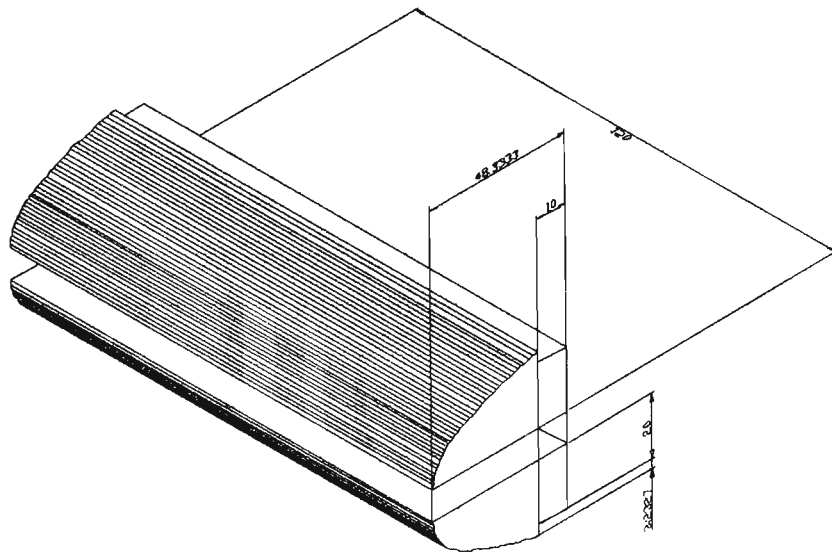
4: ER Valve, Festo HS 4/3-1/8-B;

The model of the airfoil is designed in three sections, namely, the leading and the trailing edges and the middle section. The leading and the trailing edges are solid sections, corresponding to the smaller profile of NACA 0006. A schematic drawing and photograph of the fiberglass cast model of the leading edge are shown in Figure 4.8. The nose is hinged along its entire length. When the airfoil section is needed to switch to NACA 0012 from NACA 0006, the hinge is opened to enable the required change. Similar to the leading edge, a drawing and photograph of the trailing edge are shown in Figure 4.9. The trailing edge is also hinged along its length.

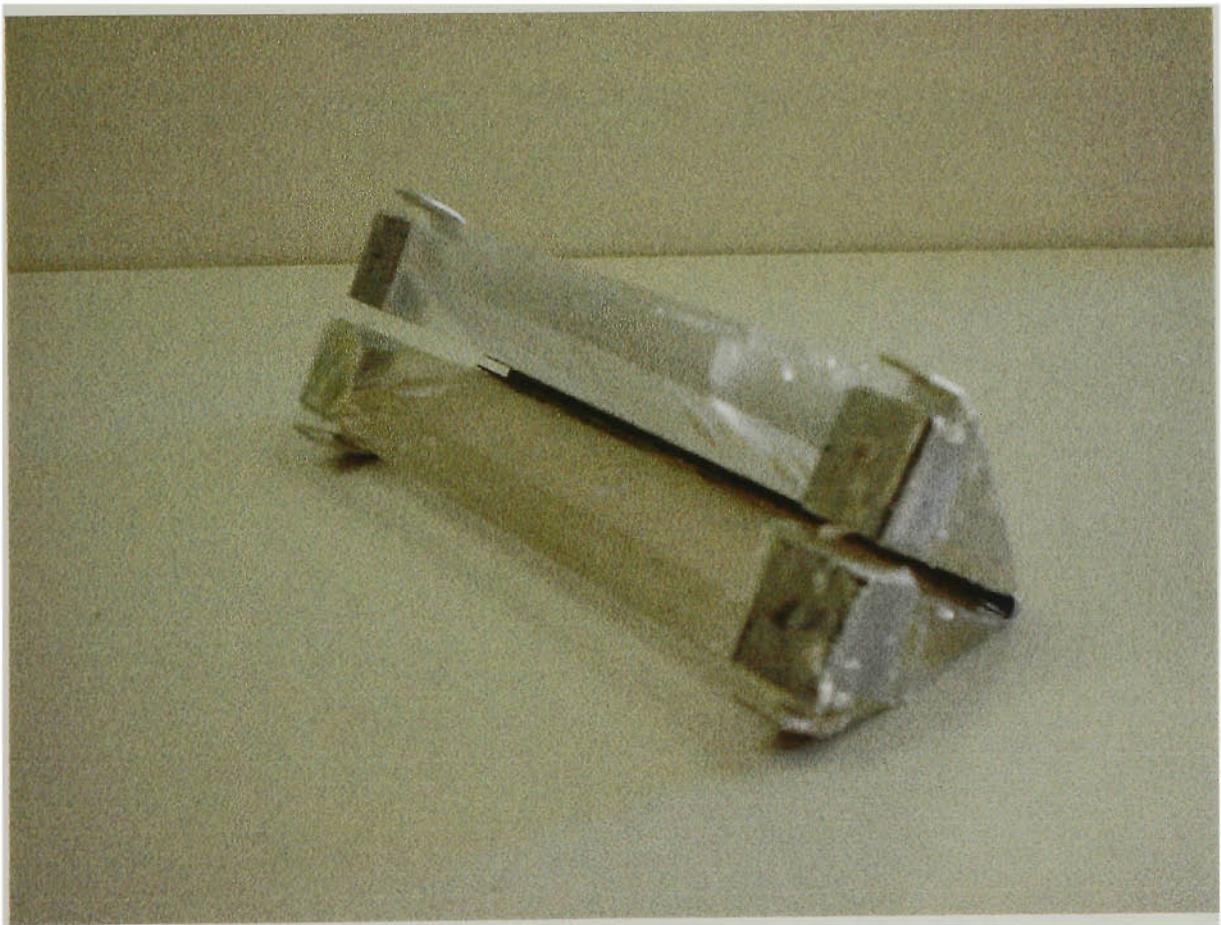
The middle section of the model is designed as a pair of two identical series of aluminium conductor plates. Each consists of 12 plates set in a non-conducting plastic strip from one end, and left free at the other end. Plastic strips extend beyond the conductor plates, and they are designed to slide into the hinges on the leading and trailing edges. Free ends of the conductor plates have non-conducting plastic shoes. The purpose of these plastic shoes is to avoid contact between the conductor plates of opposite sides when the two halves are assembled to make the middle section. Conductor plates are wired such that positive and negative charges alternate when assembled. Figure 4.10 shows the photograph of one of the two sides.

Fully assembled shapes of NACA 0006 and NACA 0012 are shown in Figures 4.11 and 4.12, respectively. NACA 0012 shape demonstrates how the leading and trailing edge hinges open to expand the profile of NACA 0006. As the hinges open, the conductor plates also move out to enlarge the cross section of the middle. The plastic shoes make sure that opposing plates do not make contact.

Figures 4.13 and 4.14 show the same two airfoil assemblies as in Figures 4.11 and 4.12, but this time with a flexible sealing jacket to contain the ER fluid. Cables connecting the voltage source are shown on the top. The fluid supply line (hidden in these pictures) is brought to the underside of the model through a hole drilled on the supporting table.

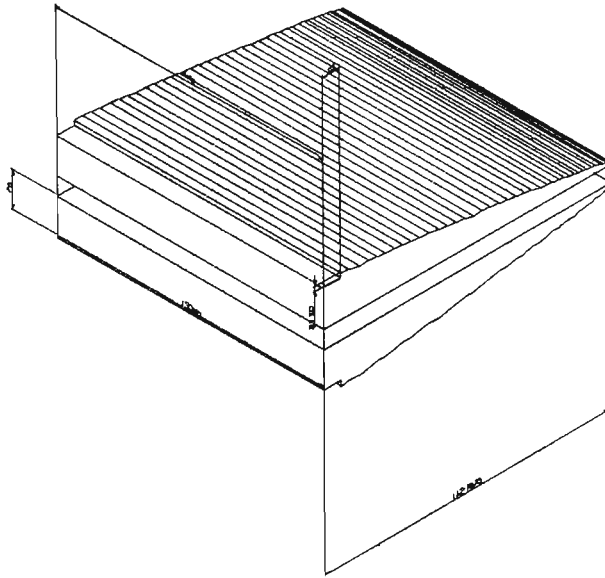


(a)

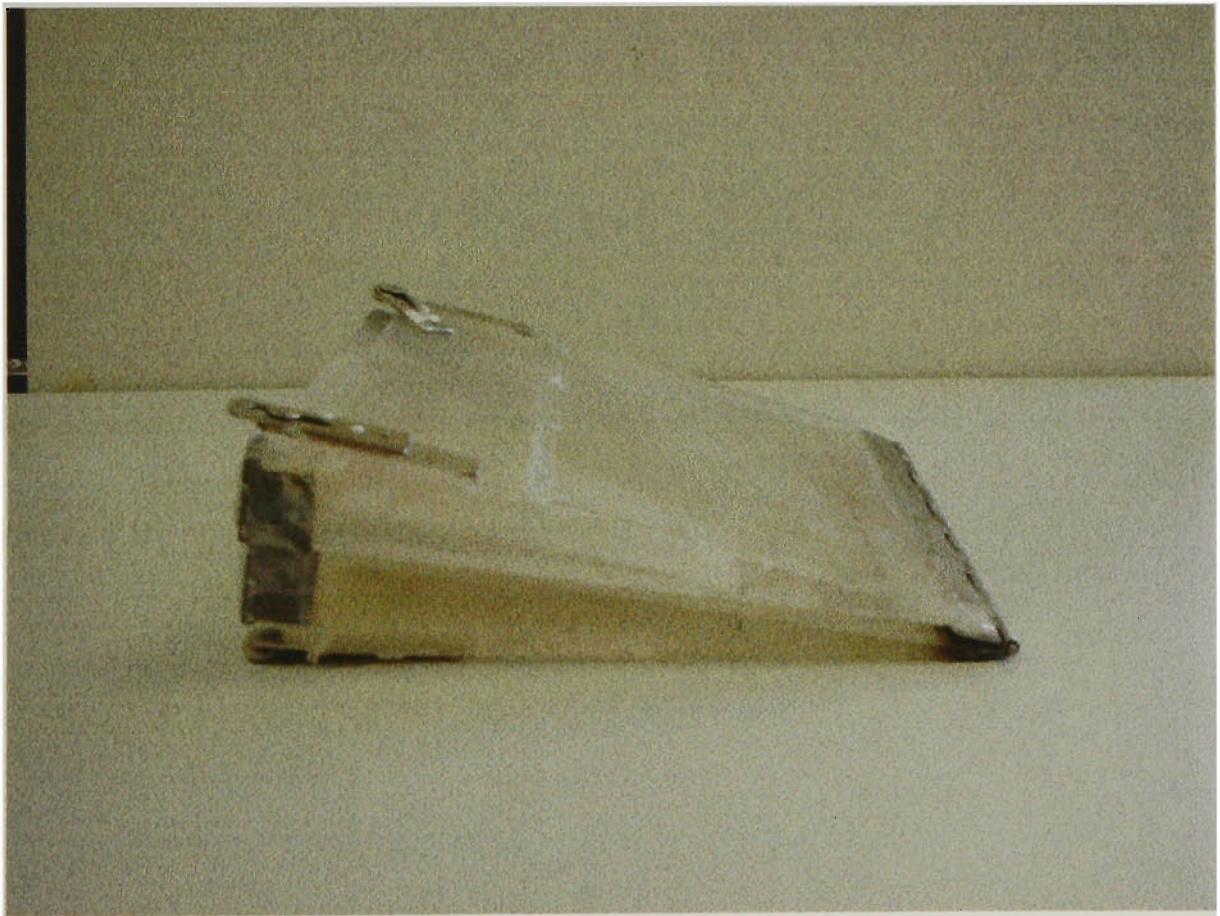


(b)

Figure 4.8. (a) Drawing and (b) photograph of the leading edge.



(a)



(b)

Figure 4.9. Same as in Figure 4.8, but for the trailing edge.

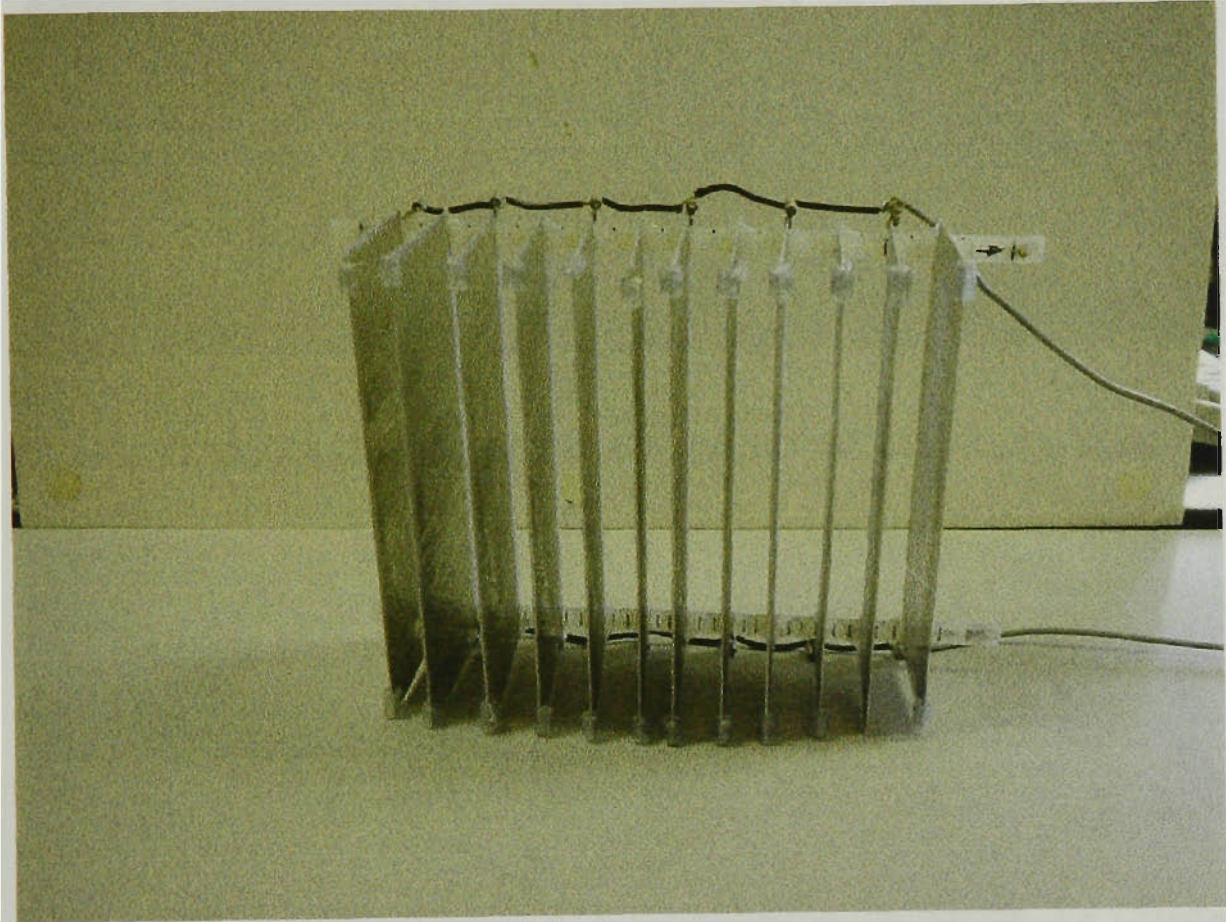


Figure 4.10. One of the conductor plate sides.

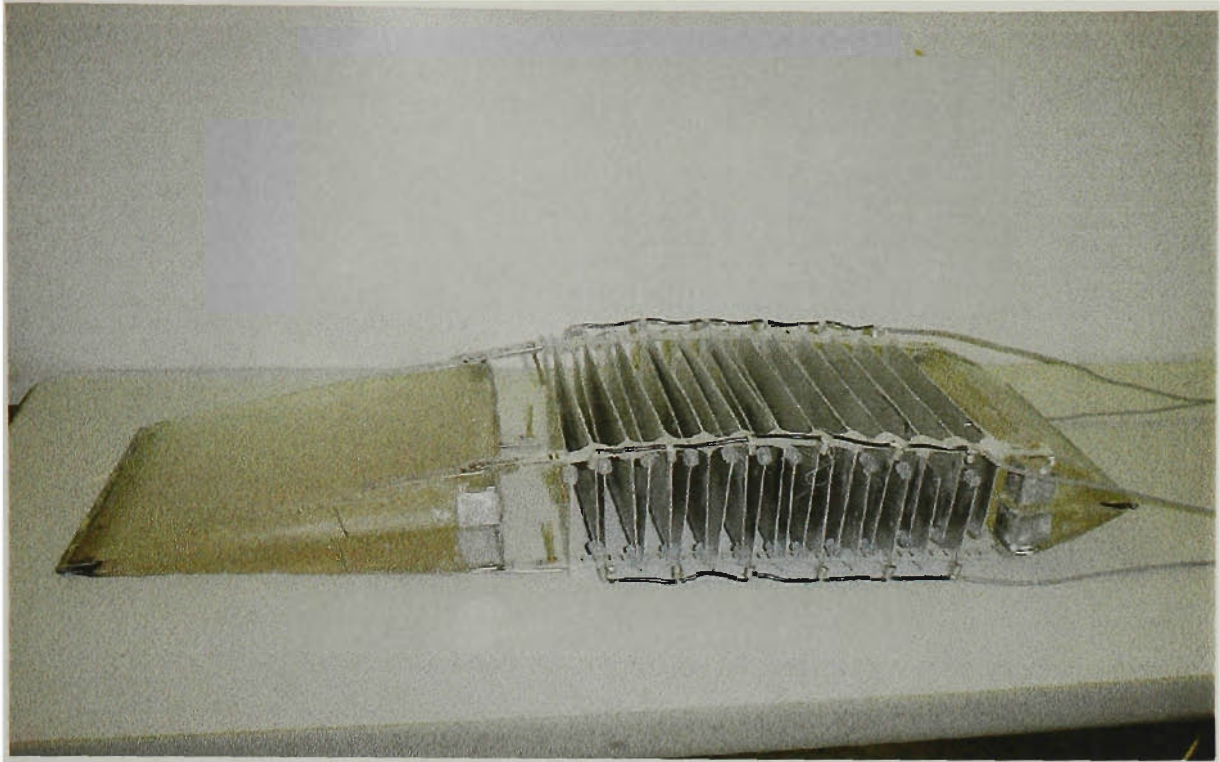


Figure 4.11. Photograph of the airfoil section NACA0006 without sealing jacket.

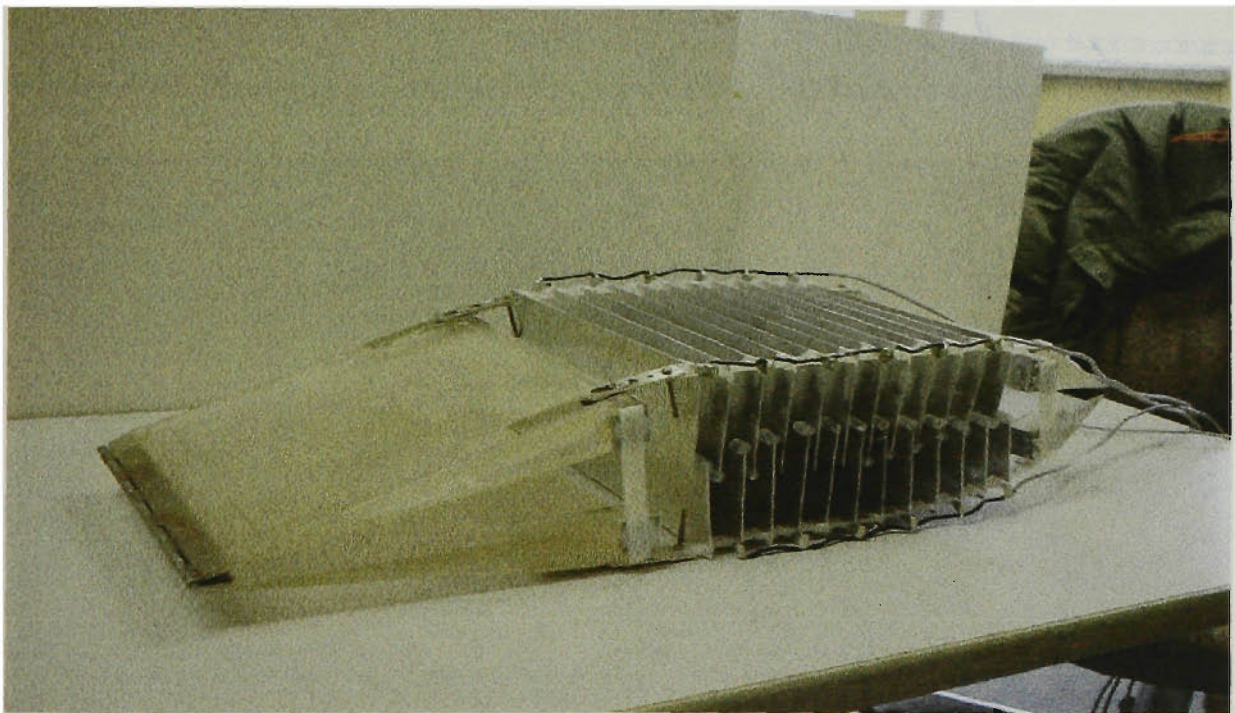


Figure 4.12. Photograph of the airfoil section NACA0012 without sealing jacket, the same assembly as in Figure 4.11, but in the fully expanded configuration.



Figure 4.13. Photograph of the airfoil section of NACA0006 with sealing jacket.

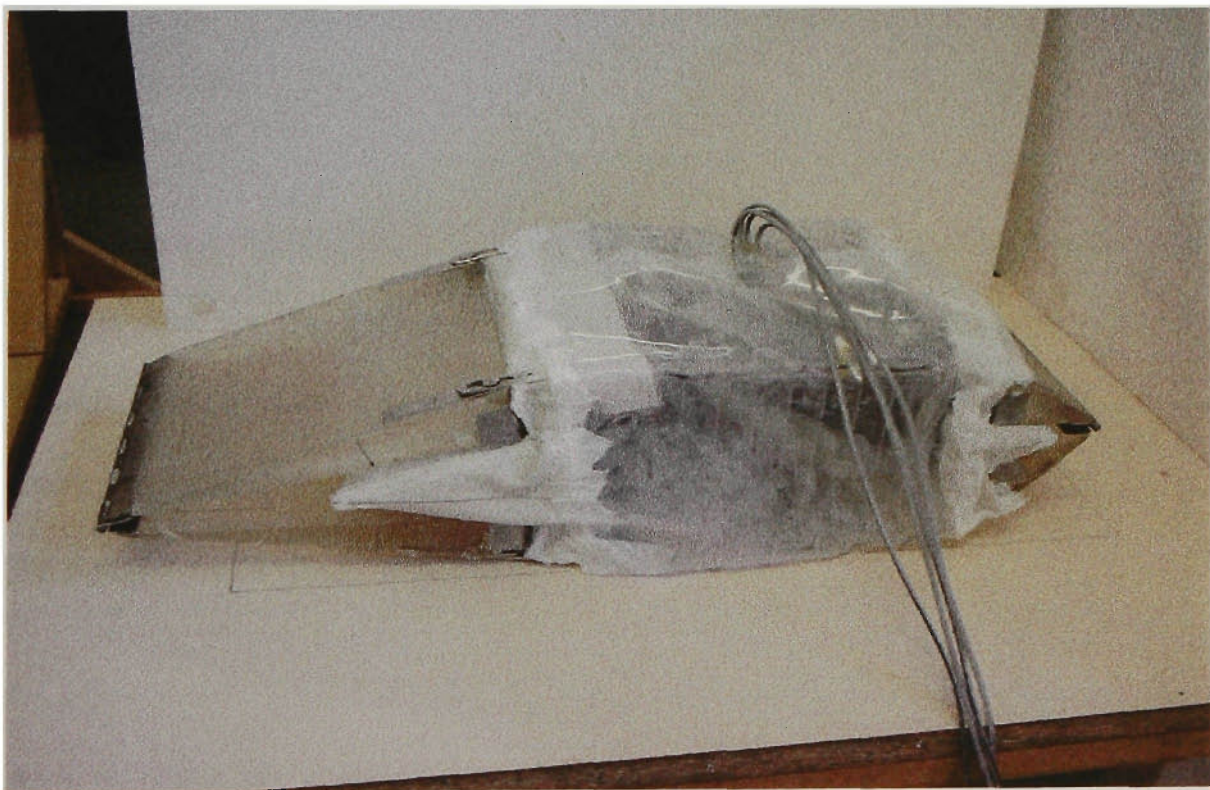


Figure 4.14. Photograph of the airfoil section of NACA0012 with sealing jacket.

The experiment consisted of starting from the smaller NACA 0006 shape. The pump was run to provide approximately 5 litres of 55% volume fraction cornstarch in mineral oil ER fluid to expand the NACA 0006 shape. The voltage source provided a nominal 0.4 kV/mm at the designed gap of approximately 15-mm between the aluminium plates. This was observed to be sufficient to change the liquid into gel to maintain the expanded NACA 0012 shape. ER fluid was drained back into its reservoir once the voltage was removed and the direction of the valve was reversed.

4.6 Conclusions

Majority of the reported ER fluid applications deal with an indirect consequence of ER effects. This indirect effect employs the phase change as a trigger to vary the dynamic response of structural components to implement the control action. A direct application is attempted in this chapter using an ER fluid to provide a shape change to an airfoil section.

At its present state, there are a number of practical issues, which need to be addressed. Two of these are: the practicality of the added mass to achieve the intended shape change, and the question of the whether the shape change will maintain integrity under significant forces. However, given the exploratory nature of the suggestion, it is felt that this chapter has a positive contribution to offer.

Chapter 5

CONCLUSIONS

Electro-Rheological (ER) fluids have the unique capability of changing their phase from liquid to a solid-like gel under the effect of an electric potential. This change is completely reversible, and it takes place within a time in the order of milliseconds. Hence, ER fluids hold great potential in engineering applications, particularly in motion control.

Research on ER fluids did not exist at Victoria University prior to this thesis project. Hence, the first objective of this thesis has been accomplished by making the essential basic research facilities available. The second objective of this thesis, namely, demonstrating the practical value of ER fluids through three particular problems, has also been achieved.

As the first of the three problems, the unique phase changing capability of ER fluids has been utilized to control excessive structural oscillations. A sloshing absorber using an ER fluid has been design and built for the purpose providing variable damping for a tuned absorber. In turn, the tuned absorber has been used to attenuate excessive resonant oscillations of a simple structure. The effect of variable damping on the structure to be controlled has also been predicted numerically. A relatively simple model was used for numerical predictions. Experiments have been performed to verify the predicted control effects. Results of this work are presented in Chapter 2.

As the second problem, an ER fluid clutch has been designed and built. Such a clutch has no moving components to control the amount of power transferred through it. Instead, the change of apparent viscosity of the ER fluid as a function of applied voltage is used to control the amount of power transfer. Chapter 3 presents the details of the design prototype and the results to support that the suggested design for an ER fluid clutch is viable. In addition, the prototype can be used to measure viscosity with some modifications.

As the third problem, an ER fluid has been used to provide a shape change to an airfoil. Chapter 4 presents the reasoning why different airfoil shapes are required during different stages of flight. Then, two standard airfoil shapes are nominated. The suggested application involves selecting either one of these two shapes by solidifying an ER fluid trapped in a cavity. Out of the three applications, this application is particularly of exploratory type. The laboratory prototype certainly demonstrates that the desired shape arrangement is possible. However, some practical problems remain before the suggested technique may be ready for application.

References

Abbott, I.H and von Doenhoff, A.E. 1958 “ **Theory of Wing Section: Including a Summary of Airfoil Data**”, Dover Publication, Inc. New York.

Anderson, J.G., Semercigil, S.E. and Turan, Ö.F. 1998 “ **A modified sloshing absorber to control structural oscillations**”. Proceedings of FEDSM'98, Washington D.C., USA

Berg, C. D., Evans, L. F. and Kermode, P. R. 1996 “**Composite Structure Analysis of a Hollow Cantilever Beam Filled with Electro-Rheological fluid**”, Journal of Intelligent Material Systems and Structures, Vol. 7, pp 494-502.

Block, H and Kelly, J. D. 1988 “ **Electro-Rheology**”, Journal Phys. D: Applied Physics, Vol. 21, pp1661-7.

Brennan, M.J., Day, M.J. and Randall, R.J. 1995 “ **An Electrorheological Fluid Vibration Damper**”, Smart Material Structure, Vol. 4, pp83-92.

Bullough, A.W., Peel, J. D., Sproton, L. J., Stanway, R. and Rodgers, L. D. 1994 “ **An ER Long-Stroke Damper for Vehicle Suspension Applications**”, Developments in Electro-Rheological Flows and Measurement Uncertainty, FED-Vol 205/ AMD-Vol 190, pp 41-49

Carlson, J. D. and Duclos, T. G. 1989 “ **ER Fluid Clutches and Brakes-Fluid Property and Mechanical Design Considerations**”, Proceeding of the Second International Conference on ER fluid, pp353-367.

Coulter, J. P. and Duclos, T. G. 1989 “ **Applications of Electrorheological Materials in Vibration Control**”, Proceeding of the Second International Conference on ER fluid, pp300-325

Etter, D. M. 1993 “**Engineering Problem Solving with Matlab**”. Prentice-Hall Inc. New Jersey

Gouzhi, Yao., Guang, M. and Tong, F. 1995, “ **Electro-Rheological Fluid and its Application in Vibration control.**”, Journal of Machine Vibration, vol(4), pp232-240.

Hara, F and Shibata, H. 1987 “**Experimental Study on Active Suppression by Gas bubble injection for earthquake induced sloshing in tanks**”, Japanese Society of Mechanical Engineers International Journal. **30** (260), pp318-323.

Hayama, S and Iwabuchi, M. 1986 “**A study on the suppression of sloshing in a liquid tank (1st Report, suppression of sloshing by means of a reversed U-tube)**”, Bulletin of Japanese Society of Mechanical Engineers, **29**(252), 1834-1841.

Housner, G. W. 1997 “ **Structural Control: Past, Present and Future**”, Smart Material System. Vol.123, p937-943.

<http://www.allstar.fiu.edu/wings31.html>

<http://handleyinnovations.com/glossary.html>

Hunt, J. P. 1979 “**Dynamic Vibration Absorbers**”. Letchworth, London: The Garden City Limited.

Jacobs, N. E. 1931 “ **Tests of Six Symmetrical Airfoils in the Variable Density Wind Tunnel**”. Technical notes National Advisory Committee for Aeronautics, Langley Memorial Aeronautical Laboratory, July, 1931. Washington.

Kermode, A. C. 1987 “ **Mechanics of Flight**”, Ninth Edition, Longman Scientific and Technical Group, UK

Muto, K., Kasai, Y and Nakahara, M. 1988 “**Experimental tests for suppression effects of water restraint plates on sloshing of a water pool**”. Transactions of the American Society of Mechanical Engineers, Journal of Fluids Engineering, 110, August issue, pp240-246.

Otani, A., Kobayashi, H., Kobayashi, N and Tadaishi, Y. 1994 “ **Performance of a Viscous Damper using Electro-Rheological Fluid**”, Seismic Engineering, ASME, Vol. 2, pp93-97.

Suresh, B. K., Buffinton, W.K. and Conners, H.G. 1994 “ **Damping and Stiffness Control In a Mount Structure Using Electrorheological (ER) Fluids**”, ASME,

Developments in Electrorheological Flows and Measurement Uncertainty, FED-Vol.205/AMD-Vol.190.

Shigley, J. E. 1986 “**Mechanical Engineering Design**”, International Edition. McGraw-Hill, Singapore.

Snowdon, J. C. 1968 “**Vibration and Shock in Damped Mechanical Systems**”. John Wiley & Sons. New York.

Tsukiji, T. and Tanaka, N. 1996, “ **Effects of Electrical Change On The Shear Stress In ER Fluid**”, ASME, Rheology and Fluid Mechanics of Nonlinear Materials, AMD-Vol.217.

Trevor, T. 1996 “ **Aeroplane General Knowledge and Aerodynamics: for private pilot licence and commercial pilot licence**”, Second Edition, Aviation Theory Center.

Truong, T. D., Semercigil, S. E. and Turan, Ö. F. 2000 “ A Variable Damping Tuned Absorber with Electro-Rheological Fluid for Transient Resonance of Light Structures”, Journal of Sound and Vibration, accepted for publication.

Winslow, M. W. 1949 “ **Induced Vibration of Suspensions**”, Journal of Applied Physics, Vol. 12, pp1137-1140

White, M. F. 1994 “ **Fluid Mechanics**”, Third Edition, McGraw-Hill, USA

Appendix A

SOFTWARE TO SIMULATE DYNAMIC RESPONSE OF A TUNED ABSORBER

A.1 Introduction

Tuned vibration absorbers are simple and effective passive vibration control devices for lightly damped resonance structures. A simple system including a tuned absorber shown earlier in Figure 2.1(a) is repeated here in Figure A.1. The primary structure to be controlled has a mass m_1 , viscous damping coefficient c_1 and stiffness k_1 , whereas m_2 , c_2 and k_2 represent the corresponding parameters of the tuned absorber. The purpose of this Appendix is to briefly introduce the numerical procedure to approximate the solution of the differential equation of motion of the system in Figure A.1. In addition, a Matlab code is made available, and an example is given to demonstrate its use.

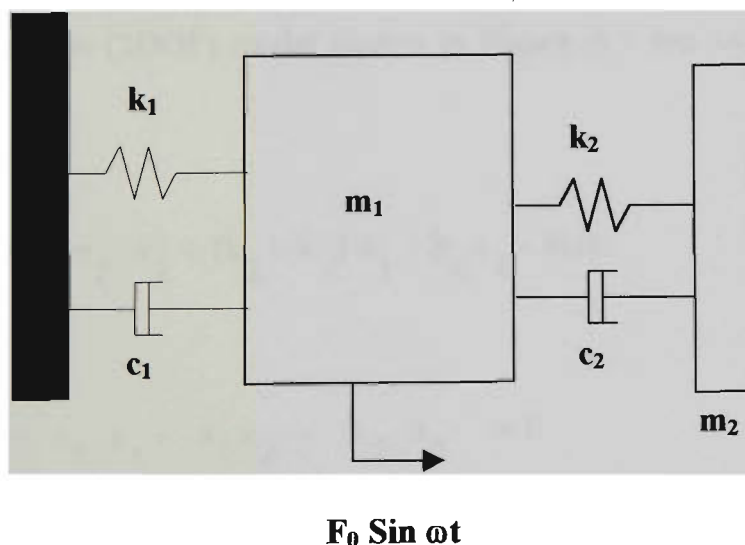


Figure A.1. A simple mechanical oscillator with a tuned absorber.

When the machine or structure to be controlled is excited at the tuning frequency, an almost perfect control effect can be obtained with an undamped absorber. The problem, however, is that the addition of the undamped absorber introduces a resonance of the combined system at a frequency lower than the tuning frequency. As the machine is started from rest, before the steady operating speed is reached, this resonance has to be traversed in transient. If not controlled effectively, such transient resonance could cause significant damage.

Including some damping in the tuned absorber reduces the adverse effects of the transient resonance significantly. The problem this time, however, is that the tuning effect is lost as the resonance amplitudes are reduced to acceptably low values. A solution to the transient problem is to have an absorber, which would have high damping in transient state and switching to no damping once the steady state is reached. This program implements such a control to solve the transient problem. This change represents the ER fluid action described in Chapter 2 of this thesis.

The 2-degree of freedom (2DOF) model shown in Figure A.1 has two differential equations of motion

$$m_1 \ddot{x}_1 + (c_1 + c_2) \dot{x}_1 - c_2 \dot{x}_2 + (k_1 + k_2) x_1 - k_2 x_2 = F(t) \quad (1)$$

and

$$m_2 \ddot{x}_2 + c_2 \dot{x}_2 - c_2 \dot{x}_1 + k_2 x_2 - k_2 x_1 = 0 \quad (2)$$

In these equations, coordinates $x_1(t)$ and $x_2(t)$ represent the absolute displacement of m_1 and m_2 , respectively. An overdot represents differentiation with respect to time. The external force is specified to be “ $F(t) = (C\omega^2) \text{Sin } \omega t$ ” to represent a rotating

unbalance during start-up of machinery, where C is an arbitrary constant. The excitation frequency ω is changed linearly up to the tuning frequency, and then, it is kept constant at the excitation frequency, to represent, respectively, the acceleration and the steady state.

A.2 Example Input

The source program here is written in Matlab (Etter, 1993) to run on a personal computer. Table A.1 represents an example input file to generate the results presented in Figures 2.5 to 2.8, on pages 23, 24, 27 and 28. These parameters are consistent with the experimental values presented in Chapter 2. The input parameters can be changed directly from the function program, “function [xdot] = vdpol(t,x)”. Lines 5 to 12 of this function program represent the damping and no damping cases, and line 13 to 20 represent the variable damping cases, i.e. damping at the transient state and no damping at the steady state. Comment lines are provided to identify each parameter. The main program uses the built-in Matlab function “ode45” to numerically integrate the equations of motion using the Runge-Kutta scheme, after calling the function program.

Table A.1 Example input with a sinusoidal excitation.

Input Parameter	SI Unit
Mass m_1	4 kg
Mass m_2	0.4 kg
Spring Stiffness k_1	1407 N/m
Spring Stiffness k_2	140.7 N/m
Damping Coefficient of Primary System c_1	0 N/cm/s
Damping Coefficient of Absorber System c_2	Ranging from 0-0.2

A.3 Example Output

Execution of the program involves calling the program file name in the Matlab command window as shown in Figure A.2. The main program is saved under the name “absorber1”, and the function program is saved under the name “2dof1”. The program listing are provided in Section A.4.

The main program generates the numerical solution from zero to 140 seconds with zero initial conditions. The output file is in a graphical format that is displayed on the screen. Histories of the displacement of the primary structure and the absorber for no damping case are shown in Figures A.3 and A.4, respectively.

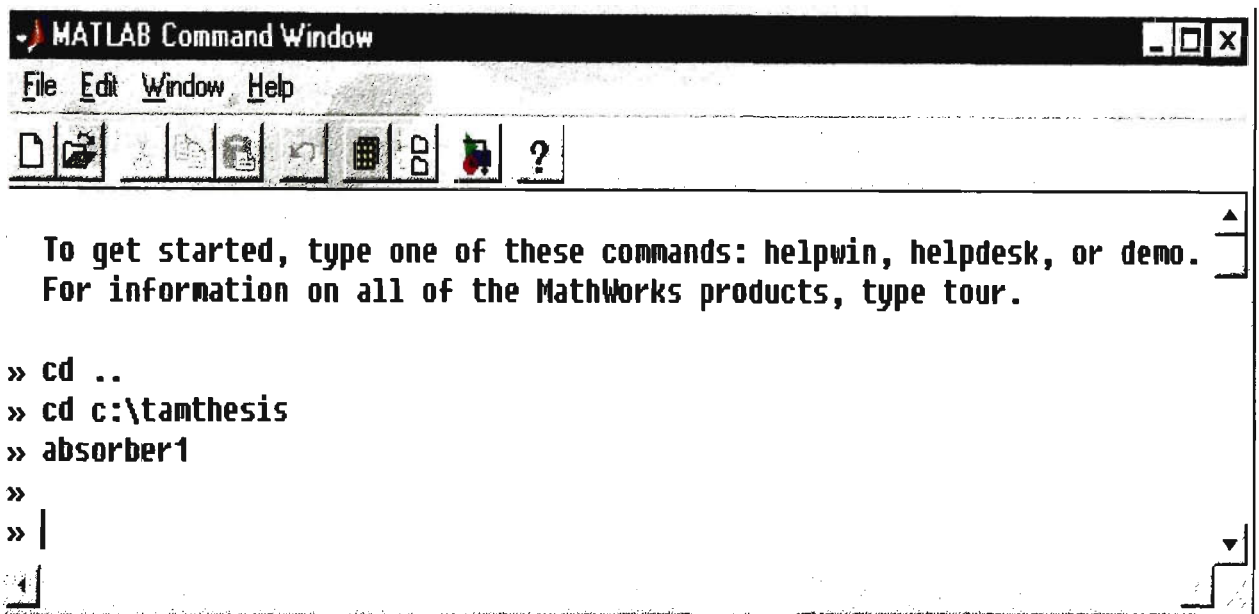


Figure A.2. Execution of the program in the Matlab command window environment.

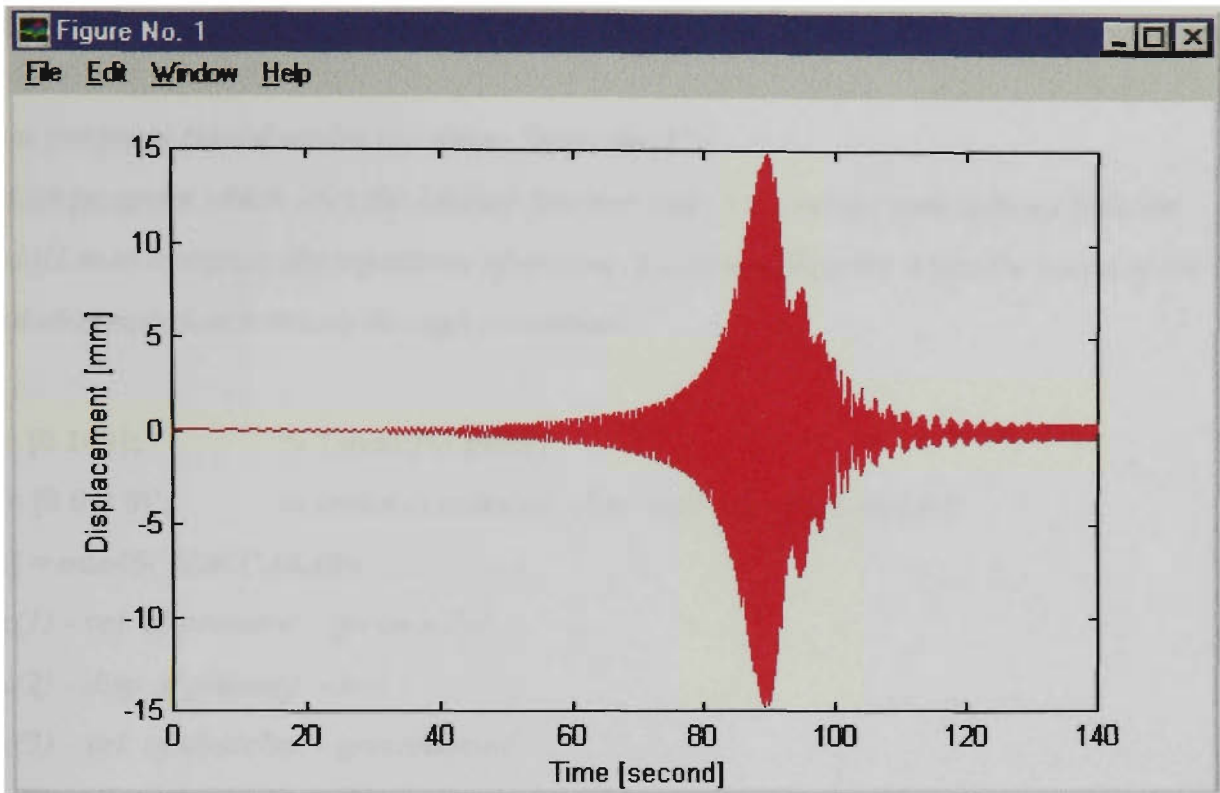


Figure A.3. Example output of the displacement history of the primary structure with no damping

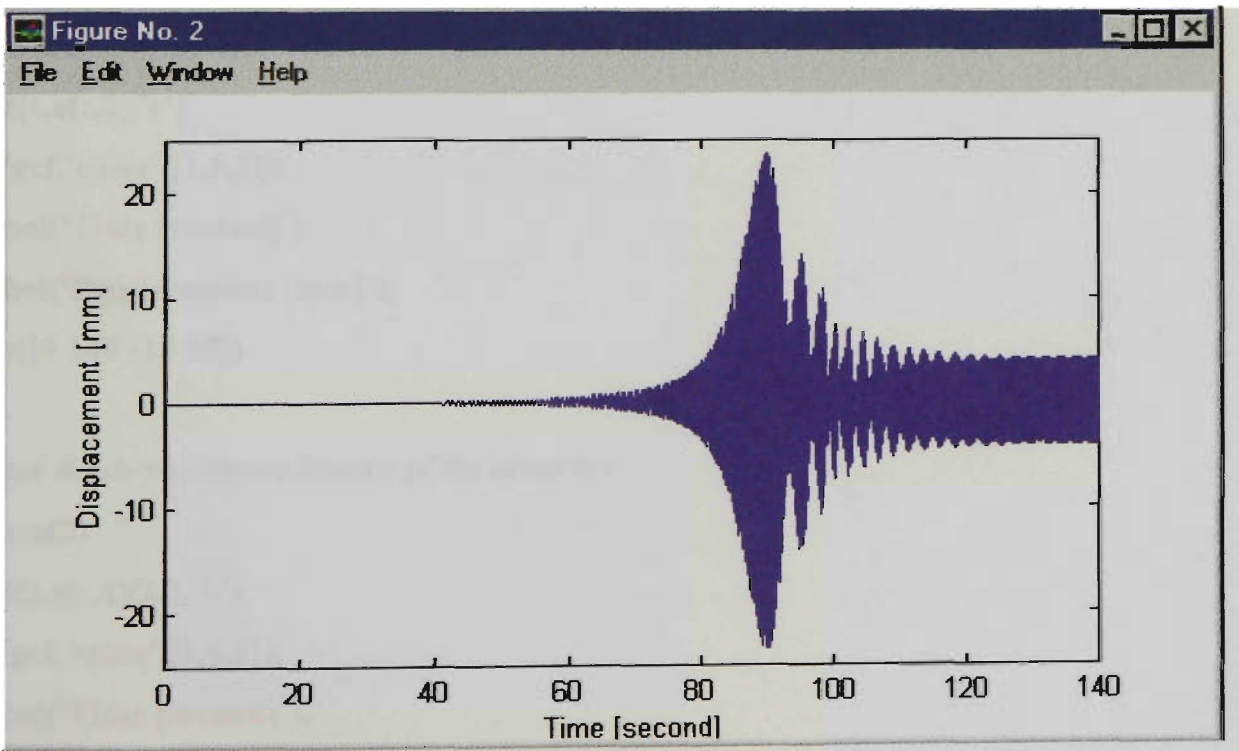


Figure A.4. Example output of the displacement history of the absorber with no damping.

A.4 Program Listing

Main program (saved under the name “absorber1”)

%Main program which uses the Matlab function ode45.m and the user defined function %2dof1.m to integrate the equations of motion of a tuned absorber when the speed of the %rotating unbalance traces through resonance.

```
t0 = [0 140];           % Tspan:[to tfinal]
x0 = [0 0 0 0]';       % initial conditions: disp. and vel. of m1 and m2
[t,x] = ode45('2dof1',t0,x0);
% x(1) - vel of primary - green/solid
% x(2) - disp of primary - red
% x(3) - vel of absorber - green/dotted
% x(4) - disp of absorber - blue
% Force Function – yellow

%plot the displacement history of the primary mass
figure(1)
plot(t,x(:,2),'r')
set(gcf,'color',[1,1,1]);
xlabel('Time [second]');
ylabel('Displacement [mm]');
axis([0 140 -15 15])

%plot the displacement history of the absorber
figure(2)
plot(t,x(:,4)/2.5,'b')
set(gcf,'color',[1,1,1]);
xlabel('Time [second]');
ylabel('Displacement [mm]');
axis([0 140 -25 25])
```

Function Program (saved as the name “2dof1”)

%Function program to describe the equations of motion, the variation of the speed of the unbalance and damping as a function of time. This program is meant to be used by Matlab function ode45.m which is called by main routine absorber1.m.

```
function [xdot] = vdpol(t,x)  
[rows,cols]=size(x);  
xdot = zeros(rows,cols);           % MxN matrix initialised with zeros.  
to=100;                          % final time for the frequency transient in seconds.  
m1 = 4;                            % Mass of primary system [kg]  
k1 = 1407;                        %Stiffness of primary system [N/m]  
w=18.75;                          % final frequency for the transient in rad/s (also the tuning freq.).  
  
zeta1 = 0.0;                       %critical damping ration of the primary system.  
c1 = zeta1*2*sqrt(m1*k1);          % Damping coefficient for zeta1.  
m2 = 0.4;                          % Mass of absorber[kg]  
k2 = 140.7;                       % Stiffness of absorber[N/m]  
  
%The following loop is only active for variable damping case  
  
% i=1:length(t);  
% if t(i) <= to;  
%   zeta2 = 0.2;                   % No voltage damping ratio  
%   c2(i) = zeta2*2*sqrt(m2*k2);   % Damping coefficient  
% elseif t(i)>= to;  
%   zeta2 = 0.02;                  % Damping ratio with 4000 Volts  
%   c2(i) = zeta2*2*sqrt(m2*k2);  % Damping coefficient  
% end
```

%Declare constant damping values for uncontrolled cases

zeta2 = 0.20; *% No-Voltage damping ratio resulting from the sloshing absorber*

c2= zeta2*2*sqrt(m2*k2); *% damping coefficient for zeta2*

%The following section is to decide on the value of the unbalance force at any time step %of integration with variable frequency. Note the multiplier 0.5 in the argument of the %ramp function until to seconds. Note the constant frequency after to.

j=1:length(t);
if t(j) < to;
force(j)=4*(w*(t(j)/to))^2*sin(w*0.5*(t(j)/to).*t(j));
elseif t(j)>to;
force(j)=4*w^2*sin(w.*t(j));
end

%Expressions for the velocity and displacement of the primary system and the absorber, %respectively, at each time step.

xdot(1) = 1/m1*(force(j)-(c1+c2)*x(1) - (k1+k2)*x(2) + c2*x(3) + k2*x(4));

xdot(2) = x(1);

xdot(3) = 1/m2*(-c2*x(3) - k2*x(4) + c2*x(1) + k2*x(2));

xdot(4) = x(3);